IGNITION DELAY TIME MEASUREMENTS OF JET, ROCKET, AND DIESEL FUEL

A Thesis

by

SULAIMAN ABDULAZIZ A ALTURAIFI

Submitted to the Office of Graduate and Professional Studies of
Texas A&M University
in partial fulfillment of the requirements for the degree of

MASTER OF SCIENCE

Chair of Committee,	Eric Petersen
Committee Members,	Waruna Kulatilaka
	Rodney Bowersox
Head of Department,	Andreas Polycarpou

August 2018

Major Subject: Mechanical Engineering

ABSTRACT

Multicomponent fuels, such as kerosene and diesel fuel, are the primary source of energy powering the engines used in the transportation sector. The study of these fuels is essential to improving engine efficiency and reduce pollutants. This efficiency improvement can be partially achieved by improving the combustion chemistry, which can potentially lead to numerous economic and environmental benefits. Several parameters affect the combustion chemistry, but one of the most important parameters is the ignition delay time of the fuel and oxidizer. The work presented in this thesis explored the ignition behavior of three fuels heavily utilized in the transportation sector.

Ignition delay times were measured for gas-phase jet fuel (Jet-A), rocket propellant (RP-1), and diesel fuel (DF-2), in a heated, high-pressure shock tube. The measurements were performed behind a reflected shock wave for each fuel in air over a temperature range of 785 to 1293 K for two equivalence ratios, ϕ = 0.5 and 1.0, at two different pressures, 10 and 20 atm. Ignition delay time was determined by observing the pressure and OH* chemiluminescence (~307 nm) at the endwall location. Measured ignition delay times for Jet-A were in agreement with the available historical data from the literature. Results showed few differences in ignition delay times between any of the three fuels over the temperature range studied. High-temperature correlations were developed to accurately predict the ignition delay times of the three fuels. The experimental measurements for Jet-A and DF-2 were modeled using several chemical kinetics mechanisms utilizing different surrogate mixtures. To the author's knowledge, this study presents the first gas-phase ignition delay time measurements for RP-1. In addition, the data presented in this thesis expand the archival data of Jet-A and DF-2 to a broader range of conditions.

ACKNOWLEDGMENTS

I owe a great deal of gratitude to my advisor, Dr. Eric Petersen, for his continuous support throughout my master's degree. I'm very grateful for the opportunity he gave me to be part of his research group, his patience in addressing any of my concerns, his nonstop motivation, and his immense knowledge. He is a true role model who inspires others by setting an example of hard work and determination. I would like to thank my committee, Professors Waruna Kulatilaka and Rodney Bowersox for their valuable support regarding this thesis. I would like to thank Dr. Olivier Mathieu for his guidance, help, and advice he provided me throughout my time here. I'm very grateful to Travis Sikes and Clayton Mulvihill for mentoring me in both my research work and my life. I would like to thank all my friends and colleagues in the Petersen research group (current and former). Last but not the least, I would like to thank my family: my parents and my brothers and sisters for supporting me throughout my life in general.

CONTRIBUTORS AND FUNDING SOURCES

This work was supervised by a thesis committee consisting of Professor Eric Petersen and Waruna Kulatilaka of the Department of Mechanical Engineering and Professor Rodney Bowersox of the Department of Aerospace Engineering.

This work was supported in part by the Qatar National Research Fund NPRP project 8-1358-2-579. The author would like to thank Dr. T. Edwards from the Air Force Research Laboratory for providing the fuels used in this work. Additional contribution was provided by the Saudi Arabian Cultural Mission in the form of scholarship funding under scholarship 465525.

TABLE OF CONTENTS

Page

LIST OF FIGURES

Page

LIST OF TABLES

Page

CHAPTER I

INTRODUCTION AND LITERATURE REVIEW

1.1 Motivation

In 2015, the world's total energy consumption was 575 quadrillion British thermal units and it is expected to rise 28% by 2040 [1]. This energy is produced mainly through sources such as coal, natural gas, renewables, and nuclear fission. The largest portion, around 33%, is produced using "petroleum and other liquid fuel sources" and it is expected to remain the largest segment in 2040. In addition, the consumption of liquid fuels is expected to rise from 95 million barrels per day to 113 million barrels per day in 2040. Thus, there is an essential need for research tailored to improve the combustion efficiency of liquid fuels, which will lead to numerous economic and environmental benefits.

The majority of liquid fuels are consumed in the transportation sector where combustion engines are utilized to extract the fuel's energy and convert it to mechanical work. A few examples of these engines are internal combustion, rocket engines, and gas turbine engines. The design of these engines relies on many factors such as heat transfer, gas dynamics, multi-phase flows, and flow turbulence. Nevertheless, the predominant factor on the overall efficiency of these engines is controlled by combustion chemistry. Usually, combustion engine designers rely on numerical simulation software packages that utilize chemical kinetics mechanisms to predict the combustion chemistry. Therefore, developing accurate kinetics mechanisms is vital to the advancement of combustion engines.

Kinetics mechanisms are hundreds, in some cases thousands, of first-order differential equations that describe species rates of change over time, i.e. a pathway of a fuel and an oxidizer

to turn into combustion products. During the combustion process, the fuel starts by decomposing to smaller molecules through various reactions. If the fuel compounds are simple, then the number of reactions can be small. However, liquid petroleum-based fuels, such as kerosene and diesel, are blends of thousands of different hydrocarbon molecules. This fact makes the kinetics mechanisms of liquid fuels complicated because there are many intermediate species and numerous possible reactions. One method of simplifying these mechanisms is to use surrogate models, which usually contain fewer numbers of hydrocarbons, to mimic the chemical and physical properties of the liquid fuel.

Developers of kinetics mechanisms typically utilize fundamental parameters, such as ignition delay time, as targets to validate their models. One device to measure ignition delay times of a gas-phase fuel/oxidizer mixture is a shock tube, but liquid fuels typically have low vapor pressures, which complicate gas-phase shock-tube experiments. One successful method to test a low vapor pressure liquid fuel is to heat the shock tube, thus increasing the vapor pressure of the liquid fuel which allows gas-phase shock-tube experiments. Another method is to use an aerosol shock tube where the multicomponent fuel is introduced into the shock tube in micro-sized droplets and tested as a heterogeneous mixture.

In this thesis, a shock tube, equipped with a heating system, was utilized to measure ignition delay times of several liquid fuels. The liquid fuels were mixed with air, and the measurements were made at elevated temperatures and pressures to mimic practical engine conditions. These measurements add to the available literature data in a global effort to create a benchmark for researchers to validate liquid fuel chemical kinetics mechanisms.

1.2 Background

1.2.1 Jet Fuel Ignition Delay Time

Jet fuels are kerosene-based distilled fuels used in military and commercial aviation. There are several types of jet fuels which are mainly classified by the distillation process and have additives such as corrosion inhibitors, fuel system icing inhibitors, and lubrication improvers. Jet-A is the commercially used jet fuel for the aviation industry in the United States, while the rest of the world uses Jet-A-1. JP-8 (jet propellant) is another type of jet fuel which has a Jet-A fuel base with three military specified additives: anti-static additive, fuel system icing inhibitor, and a corrosion inhibitor. Usually, jet fuel compositions differ from one refinery to another and even from batch to batch. However, the National Jet Fuels Combustion Program led by the Federal Aviation Administration, U.S. Air Force Research Laboratory, and NASA classified jet fuels into three categories based on three selected combustion related properties: flash point, viscosity, and aromatics content. The three categories and their military POSF number are A-1 (POSF10264), A-2 (POSF1025), and A-3 (POSF10289). A-1 is the "best case" jet fuel with a low flash point, viscosity, and aromatics which is very similar to JP-8. A-2 is the "average" properties of a jet fuel which is Jet-A. A-3 is the "worst case" jet fuel which is a fuel very similar to JP-5 [2, 3]. Figure 1 and Table 1 shows selected properties of the three categories.

Table 1: Properties of jet fuels [3, 4].

Jet Fuel	Molecular Formula	Molecular Weight	Flash Point (℃)	Density (kg/L)	Heat of Comb. (MJ/Kg)	H Content (%mass)	H/C Ratio
A-1	$C_{10.8}H_{21.8}$	152	42	0.780	43.2	14.26	1.99
A-2	$C_{11.4}H_{21.1}$	159	48	0.803	43.1	13.86	1.91
A-3	$C_{11.9}H_{22.6}$	166	60	0.827	43.0	13.68	1.89

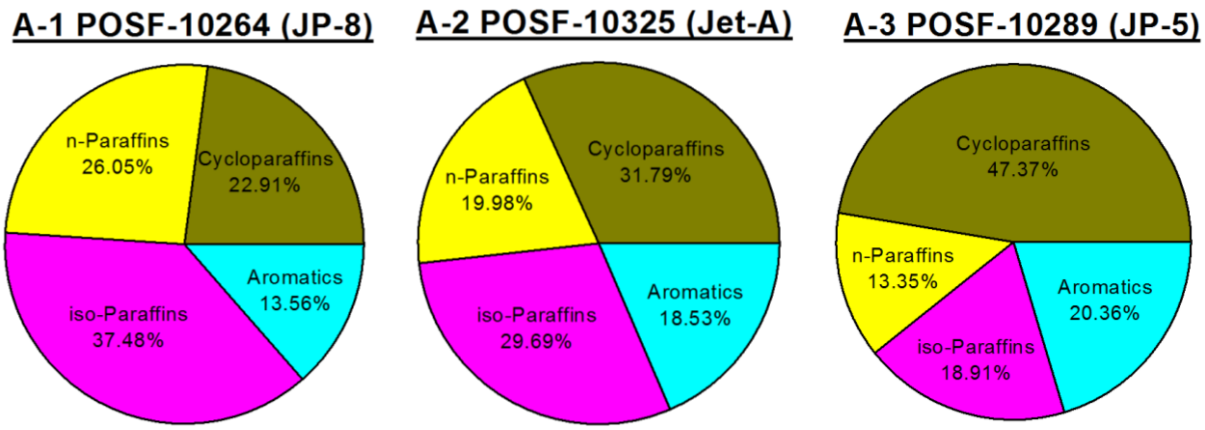

Figure 1: Jet fuels composition [3].

Although the ignition delay time of jet fuels has been under investigation for several years, there is still a need for more experimental data to cover a broader range of conditions. The first shock-tube study of jet fuel ignition was conducted in 2007 by Dean et al. [5]. They used a heated shock tube to measure the ignition delay time of Jet-A/air mixtures at equivalence ratios of ϕ = 0.5, 1.0, and 2.0; pressures of 8.5 atm; and a temperature range of 1000-1700 K. In 2008, Vasu et al. [6] utilized a heated shock tube to measure ignition delay time of two types of jet fuels, Jet-A and JP-8, at two equivalence ratio of 0.5 and 1.0 and under high-pressure conditions of 17-51 atm. Vasu et al.'s study was for a wide range of temperature of 715-1229 K which allowed them to access the negative-temperature-coefficient (NTC) region. Subsequently, Kumar et al. [7] used a rapid compression machine (RCM) to test the same two jet fuels tested by Vasu. They expanded the ignition delay time measurements to include a broader equivalence ratio range of 0.42-2.26 and reached lower temperatures of around 650 K. In 2012, Wang et al. [8] investigated the auto-ignition of five compositionally-distinct jet aviation fuels. His investigation included Jet-A, a blend of Jet-A with JP-8 additive package, two Fischer–Tropsch (F–T) jet fuels, S-8, and Shell GTL. Wang and coworkers found in their study that the ignition delay times of these fuels for the high-temperature region were indistinguishable. However, they noticed that the ignition delay times

diverge in the NTC and low-temperature regimes. A couple of years later, Zhukov et al. [9] studied the ignition delay time of Jet-A in air at two pressures of 10 and 20 atm and three equivalence ratios of 0.5, 1.0, and 2.0 but only included the high-temperature region of 1040-1380 K.

In 2017, Davidson et al. [10] measured the ignition delay time of three types of jet fuels: JP-5, JP-8, and Jet-A. Their measurements included the high-temperature region of 1000-1400 K but for a wide range of pressure of 6-60 atm. They used an aerosol shock tube for the low-pressure measurements (less than 10 atm) and a heated shock tube for the high-pressure measurements. In their study, they noted an indistinguishable difference in ignition delay time when varying the equivalence ratio between 0.85-1.15. Also, they found that the ignition delay times for the three fuels were very similar and provided an Arrhenius expression correlation that predicted the ignition times. In the same year, De Toni et al. [11] studied the ignition behavior of Jet-A-1 fuel using both a rapid compression machine (RCM) and a heated shock tube. They expanded the available experimental data to leaner conditions to reach an equivalence ratio of 0.3 and a wide range of temperature of 670-1200 K. In their study, De Toni and coworkers noticed that the negative-temperature-coefficient (NTC) was limited to the range of 700-870 K and the remaining temperature range showed an Arrhenius-like behavior. In addition, De Toni et al. reported that their RCM experiments showed a two-stage ignition behavior for temperatures below 760 K. In 2018, both Burden et al. [12] and Shao et al. [13] conducted ignition delay time experiments on three types of Jet fuels: A-1, A-2, and A-3. Burden used a heated shock tube and a constant-volume spray combustion chamber to find that the ignition delay times of the three fuels were similar in the high-temperature region but observed a small deviation in the NTC and low-temperature regimes. Table 2 shows a summary of the historical ignition delay time studies for jet fuels.

Table 2: Summary of literature studies for jet fuels/air ignition delay time [5-14].

Year	Author	Facility	Fuels	ϕ	Pressure	Temperature
2007	Dean[(1)]	Heated ST	Jet-A	0.5, 1.0, 2.0	8.5 atm	1000-1700 K
2008	Vasu[(2)]	Heated ST	Jet-A, JP-8	0.5, 1.0	17-51 atm	715-1229 K
2010	Kumar[(3)]	RCM	Jet-A, JP-8	0.42-2.26	7, 15, 30 bar	650-1100 K
2012	Wang[(4)]	Heated ST	Jet-A, JP-8, S-8, Shell GTL, Sasol IPK	0.25-1.5	8-39 atm	651-1381 K
2014	Zhukov[(5)]	Heated ST	Jet-A	0.5, 1.0, 2.0	10, 20 atm	1040-1380 K
2015	Zhu[(2)]	Heated ST	JP-8 and 15 alternative fuels	0.25-2.2	2-8 atm 16-44 atm	1047-1520 K
2017	Davidson[(2)]	Aerosol ST	Jet-A, JP-8, JP-5	0.85-1.15	6-60 atm	1000-1400 K
2017	De Toni[(6)]	RCM Heated ST	Jet-A-1	0.3-1.13	7-30 bar	670-1200 K
2018	Burden[(4)]	Heated ST CVSCC	Jet A (A-1, A-2, A-3)	1.0	1-8 MPa	620-1310 K
2018	Shao[(2)]	Heated ST	Jet A (A-1, A-2, A-3)	0.5-1.0	12-40 tm	1000-1400 K

(1) General Electric Global Research Center, USA
(2) Stanford University, USA
(3) Case Western Reserve University, USA
(4) Rensselaer Polytechnic Institute, USA
(5) Moscow Institute of Physics and Technology, Russia
(6) Federal University of Santa Catarina, Brazil

1.2.2 Rocket Fuel Ignition Delay Time

Rocket fuels, usually called rocket propellants, are kerosene-based fuels typically used to power rocket engines. The most common rocket fuel is RP-1 which is used with liquid oxygen as an oxidizer to power rocket engines such as Saturn V [15]. In recent years, the effort to reduce the sulfur content in RP-1 has resulted in a sulfur limit reduction from 500 to 30 ppm. However, a new grade of rocket propellant was developed with ultra-low sulfur (less than 0.1 ppm) which is called RP-2 [16]. There are several types of RP-1 and RP-2 where minor variations are performed to enhance selected properties. These types are usually classified by a military POSF number.

There have only been a few gas-phase ignition delay time studies conducted on rocket fuels. In 2017, Davidson et al. [10, 17] conducted two ignition delay time studies on two types of RP-2, POSF 7688 and POSF 5433. In their first study, the Stanford group used a heated shock tube to measure the ignition delay time at an equivalence ratio of 1.0 and a pressure of 13 atm. They reported similar ignition delay times for temperatures above 1000 K and a small difference in the low-temperature region. In a second study, Davidson et al. [17] used an aerosol shock tube to test the two fuels at a pressure of 10 atm and an equivalence ratio range of 0.8-1.2. It was reported that the effect of varying the equivalence ratio was indistinguishable for that range. In 2018, Xu et al. [4], developed a model for the high-temperature combustion of real multicomponent fuels. They measured few ignition delay times for two types of RP-2 to validate their model. The measurements were carried out using a heated shock tube at a pressure of 11.2 atm and an equivalence ratio of 1.0. A summary of the condition of these studies is presented in Table 3, and the ignition delay times are plotted in Figure 2.

Table 3: Summary of literature studies for rocket fuels/air ignition delay time [4, 10, 17, 18].

Year	Author	Facility	Fuels	ϕ	Pressure	Temperature
2018	Xu[(1)]	Heated ST	RP-2	1.0	11.2 atm	990-1250 K
2017	Davidson[(1)]	Aerosol ST	RP-2	0.8-1.2	10 atm	1000-1200 K
2017	Davidson[(1)]	Heated ST	RP-2	1.0	13 atm	700-1250 K
2014	Zhang[(2)]	Heated ST	RP-3	0.2, 1.0, 2.0	1-20 atm	650-1500 K

(1) Stanford University, USA
(2) Institute of Atomic and Molecular Physics, China

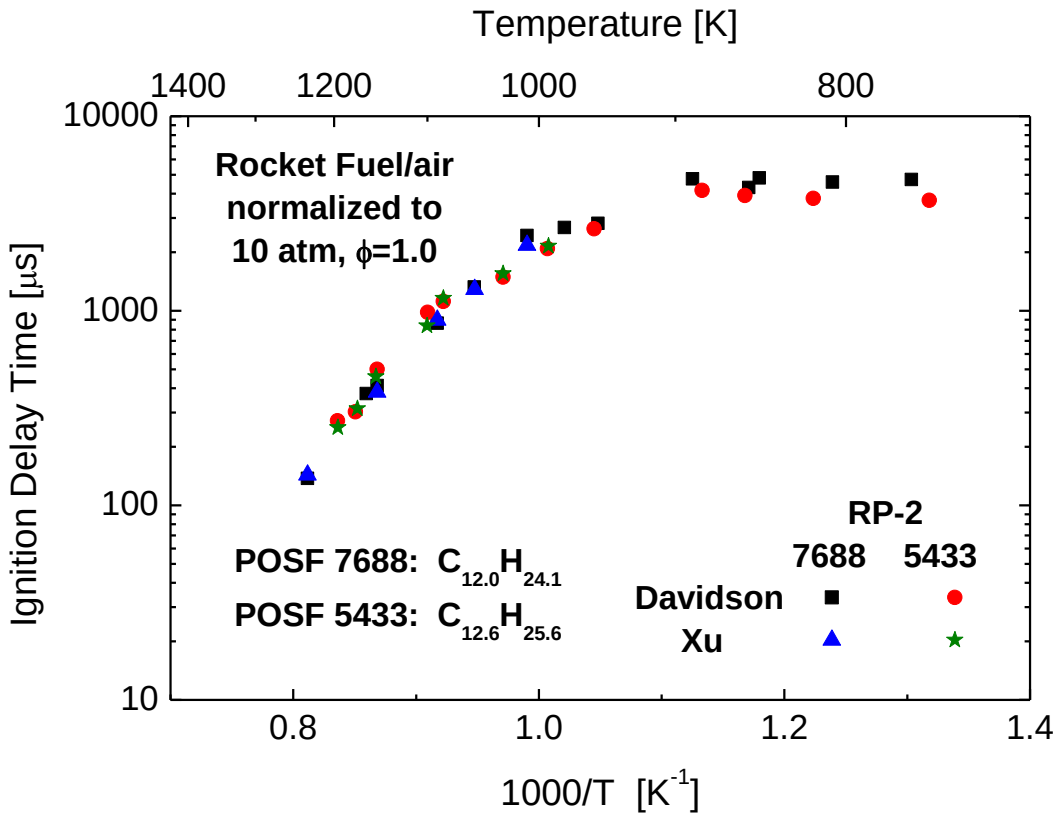

Figure 2: Available shock tube ignition delay times in the literature for rocket fuel in air, normalized to 10 atm using P^{-1} [4, 10, 17].

1.2.3 Diesel Fuel Ignition Delay Time

Diesel fuel ignition has been under investigation through the past century. The first to measure the ignition delay time for diesel fuel is Wolfer in 1938 [19]. Since then, several ignition delay time tests have been conducted using constant volume combustion apparatus [20-22], rapid compression machine (RCM) [23, 24], continues flow reactors [25], and shock tubes [10, 26-29].

In 2009, Haylett et al. [27] used an aerosol shock tube to investigate the ignition behavior of a diesel fuel (DF-2) in 21% O_2 diluted in argon. These experiments were conducted at a pressure of 2-8 atm, an equivalence ratio of 0.3-1.35, and a temperature range of 900-1300 K. After a couple of years, the same author [26] conducted another study to include several diesel fuels. He measured the ignition behavior of US DF-2, Europe DF2, Low aromatic DF2, and High aromatic DF2. The difference in ignition times for these fuels was small with fuels having larger derived cetane number (DCN) exhibiting shorter ignition delay times. Penyazkov et al [29] utilized a heated shock tube to investigate the ignition delay time of a commercial diesel fuel No. 2 in air at high temperatures. His measurements span a pressure range of 4.7-10.4 atm and an equivalence ratio of 0.5-2.0. In 2014, Gowdagiri et al. [28] conducted ignition delay time measurements using a heated shock tube for a military diesel fuel (F-76) and an alternative hydro-processed renewable diesel fuel derived from hydroprocessing algal oils (HRD-76). He found that the ignition delay times of the two fuels were indistinguishable at high temperatures (above 1000 K) while HRD-76 produced faster ignition time than the military diesel fuel at low-temperature. Gowdagiri argued that this is due to the large fraction of n-paraffins and the lack of aromatics in HRD-76. In addition, he presented an Arrhenius model of the ignition delay time that includes the effect of the fuel derived cetane number (DCN). In 2016, Kukkadapu et al. [30] conducted an auto ignition study using an RCM on two types of diesel fuels, ultra-low-sulfur diesel (ULSD) #2 and research diesel FD9A.

The two fuels had similar cetane ratings and similar ignition delay times at high to intermediate temperatures but exhibit varying ignition delay times at low-temperature regime. The author attributed this difference to the sensitivity of the chain branching reactions at that range of temperature. In, 2017, Davidson el al [10] measured the ignition delay time of two types of diesel fuel, DF-2 and F-76, in an aerosol shock tube and a heated shock tube. The measurements were at a high temperature of 1000-1400 K and a pressure range of 6-60 atm. Table 4 summarizes a few recent diesel fuel ignition studies.

Table 4: Summary of the recent studies for diesel fuels ignition delay time [10, 24, 26-30]

Year	Author	Facility	Fuels	ϕ	Pressure	Temperature
2017	Davidson	Heated ST Aerosol ST	DF-2 F-76	0.85-1.15	6-60 atm	1000-1400 K
2016	Kukkadapu	RCM	ULSD#2, F-76, FD9A	0.5-1.02	10, 15, 20 bar	678-938 K
2014	Gowdagiri	Heated ST	F-76, HRD-76	0.5, 1.0	10, 20 atm	671-1266 K
2012	Haylett	Aerosol ST	US DF-2 Europe DF2 Low aromatic DF2 High aromatic DF2	0.1-2.0	1.7-8.6 atm	838-1381 K
2009	Penyazkov	Heated ST	DF-2	0.5-2.0	4.7-10.4 atm	1065-1838 K
2009	Haylett	Aerosol ST	DF-2	0.3-1.35	2.3-8.0 atm	900-1300 K

1.3 Scope and Organization of This Thesis

This study aimed to establish a reliable method of testing heavy, multicomponent fuels in a shock-tube facility. These fuels are in the liquid-phase under room temperature and pressure conditions. A new heating system has been installed previously to allow shock-tube testing of liquid fuels. However, a procedure to conduct shock-tube experiments for liquid fuels was not established, and this study aimed to address this concern. Three liquid fuels were identified to conduct high-pressure shock-tube experiments. The ignition delay times of these fuels were obtained under practical engine conditions. The new set of data can be used as validation targets for multicomponent fuels kinetics mechanisms.

Chapter II describes the experimental facility, the new heating system, the emission diagnostics setup, ignition delay time measurement method, mixture preparation procedure, and the method used to model the shock-tube data. Chapter III discussed the ignition delay time measurements for baseline fuels (n-pentane, n-octane, and n-nonane) and multicomponent fuels (Jet-A, RP-1, and DF-2). Correlations to predict the high-temperature ignition of the multicomponent fuels are provided. In addition, predictions from several kinetics mechanisms are compared with the shock-tube data. Chapter IV presents a summary of the thesis and suggests future work. Appendix sections present the raw data for all ignition delay time experiments conducted in this study.

CHAPTER II

METHODOLOGY

2.1 Shock-Tube Facility

This study has been performed using the High-Pressure Shock-Tube at Texas A&M University. The stainless steel shock tube has a 4.72-m long driven section with an inner diameter of 15.24 cm and a 2.42-m driver section with an inner diameter of 7.62 cm. A diaphragm separates the two sections. A separate 12-L stainless steel mixing tank is used to prepare fuel/oxidizer mixtures. The mixing tank and the driven section are connected via a stainless steel manifold. A vacuum system consisting of a roughing pump and a turbo-molecular pump is used to vacuum the shock tube prior to performing experiments. Then, a specific amount of fuel/air mixture is drawn from the mixing tank and introduced into the driven section. Next, the driven section is pressurized, typically with helium gas, until the diaphragm breaks. The difference in pressure creates a shock wave (usually called incident shock) that travels through the driven section elevating the temperature and pressure of the fuel/oxidizer mixture. When the shock wave hits the driven section endwall, it reflects back (usually called reflected shock) and travels back upstream, causing further elevation in temperature and pressure to the desired test conditions, beginning the experiment. At this moment, the gas around the endwall section is stationary due to the balance of the incident and reflected shocks' momentums. Several windows at the endwall section allow absorption/emission diagnostics of the high-temperature fuel/oxidizer mixture. Shortly after that (typically in the order of 2-5 ms) the expansion wave arrives at the driven section endwall decreasing the temperature and pressure and ending the experiment. A schematic of the shock tube system is presented in Figure 3, and a full description of the shock tube can be found in [31].

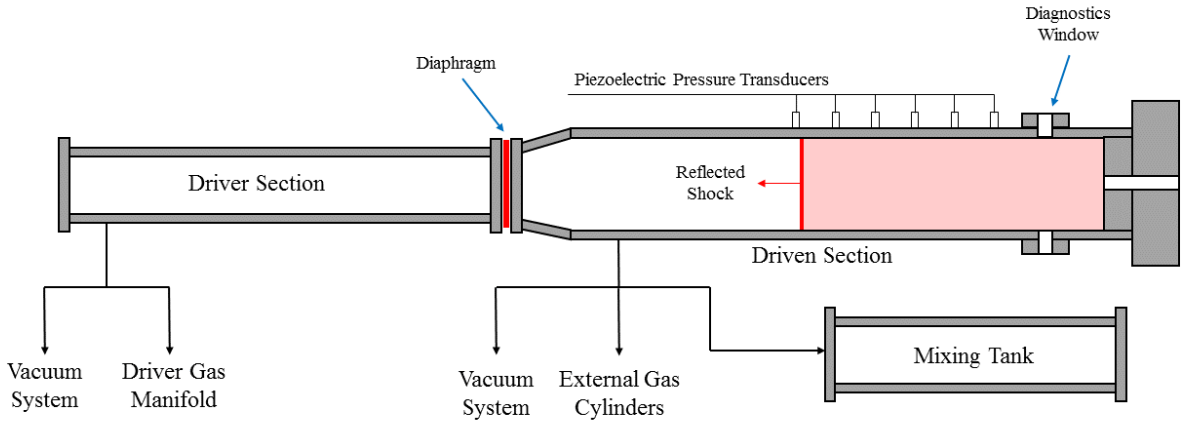

Figure 3: Schematic of the shock-tube setup.

Two types of diaphragms were used in this study, polycarbonate and aluminum diaphragms, which produced 10 and 20 atm respectively. Helium was used as the driver gas to burst the diaphragms. To achieve longer test times, 5-20% of N_2 in He was used as the driver gas as per the method of Amadio et al. [32]. Six PCB pressure transducers (Model 113B22), approximately equally spaced, located along the driven section were used to determine the shock velocity as it propagated along the driven section. Incident shock speed was calculated by linearly extrapolating the shock velocities to the end wall position. A turbomolecular pump was used to pump down the driven section to a pressure of ~1×10^{-5} torr prior to each experiment. A thermocouple was placed at the endwall to determine the temperature of the mixture prior to the shock. Reflected-shock temperature and pressure were calculated using normal shock relations and thermodynamic data. For Jet-A, thermodynamic data were taken from the Burcat and Ruscic database [33]. For RP-1, thermodynamic data were taken from the recommended values of MacDonald et al. [34] which is based on the surrogate mixture of Huber et al. [16]. For DF-2, the surrogate recommended by Pei et al. [35] which is composed of 77% n-dodecane and 23% m-xylene, was utilized.

2.2 Heating System

This section presents a recap of the high-pressure shock tube heating system. This work was conducted by Rebagay, and more details are provided in her thesis [36].

To allow low-vapor-pressure fuel experiments, the high-pressure shock tube was equipped with a heating system. The shock tube was fitted with five heating jackets and a heating tape around the endwall section. The heating tape was added to compensate for the heat loss through the endwall plate. In addition, the mixing tank has been fitted with three heating jackets. Fiberglass insulation was used to cover several bare spots to reduce heat loss. Each heating jacket was controlled by a separate temperature controller. The manifold connecting the mixing tank and the shock tube was wrapped with heating tapes to ensure no condensation occurred during the filling process. The heating jackets were supplied by BriskHeat, which can reach up to 200°C, and the heating taps were supplied by omega and are rated up to 900°F. Several temperature calibration measurements were conducted to ensure uniform temperature distribution along the driven section. Figure 4 shows the temperature distribution along the final 3 m of the driven section. A uniform temperature distribution of ±1 °C was achieved for the set-point temperatures of 50, 75, and 100 °C. However, for the 150 °C temperature set-point, a uniform temperature distribution of ±2 °C has been achieved. These uniformity distributions are for the last 3 m of the driven section, and a larger temperature drop is present near the diaphragm section.

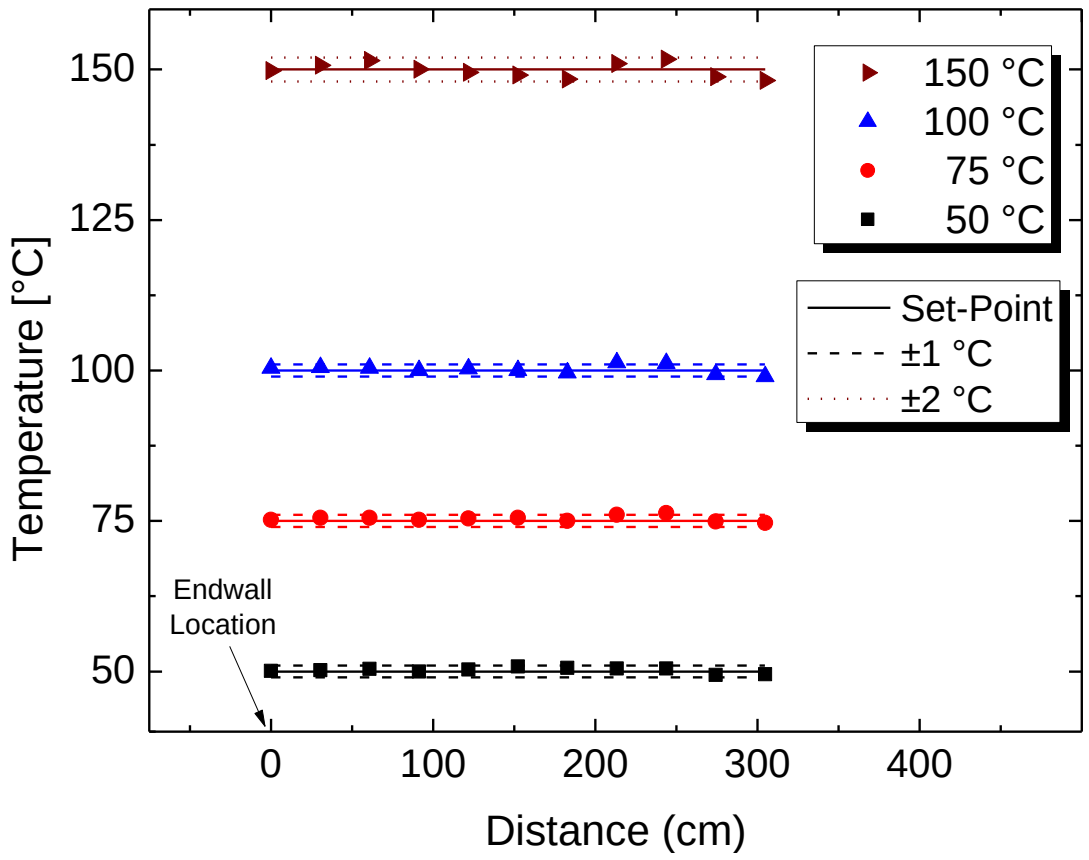

Figure 4: Temperature distribution along the driven section for several temperature set-points [36].

2.3 Emission Diagnostics Setup

During the combustion process, the transition of the electronically excited hydroxyl radical (OH*) to its ground state produces ultraviolet radiation at a wavelength of ~307 nm [37]. The emission of light from this radical is spontaneous and usually used to define the initiation of the combustion process. In this study, a diagnostic setup, shown in Figure 5, was implemented to observe OH* during shock-tube experiments. The setup consists of two photomultiplier tubes aligned to have direct visual access to the shock tube via window ports at the sidewall and endwall locations.

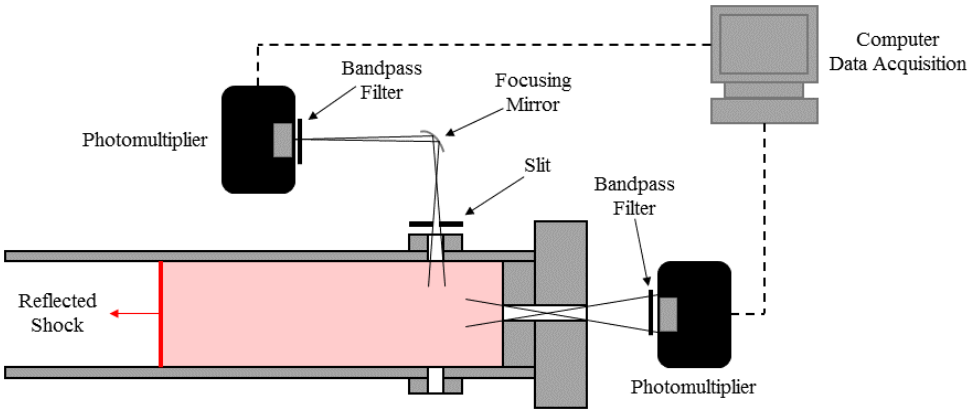

Figure 5: Schematic of the emission diagnostics setup.

2.4 Measuring Ignition Delay Time

In this study, ignition delay time was defined as the time from the arrival of the incident shock wave at the endwall to the time of the steepest rise of OH* extrapolated to the baseline. Ignition delay times were measured using a PCB pressure transducer flush to the end wall and OH* chemiluminescence near 307 nm. The pressure transducer was used to determine time zero of the ignition delay time by monitoring the sharp increase in pressure corresponding to the arrival of the incident shock wave at the endwall. On the other hand, a photomultiplier tube (Hamamatsu 1P21) and a UV bandpass (310-nm center and 10-nm FWHM) filter located at the endwall were used to record OH* time histories. The extrapolation of the deepest slope to the baseline on the OH* signal is the time corresponding to the ignition of the fuel/oxidizer mixture. Figure 6 shows a representation of an ignition delay time experiment. The overall estimated uncertainty in the ignition delay times is around ±20%, which is mainly due to the uncertainty in the incident-shock velocity.

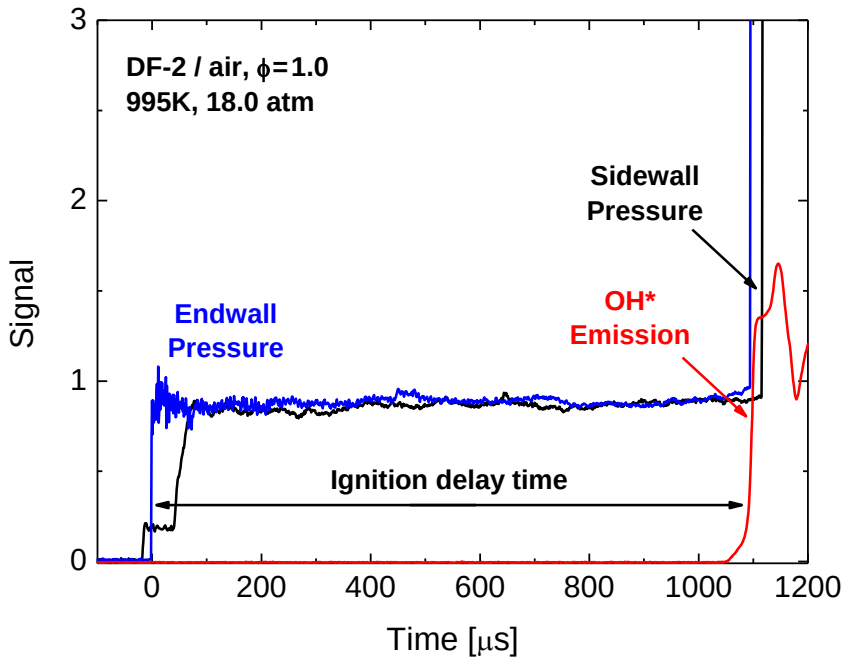

Figure 6: Representation of a sample ignition delay time experiment.

2.5 Fuel/Air Mixture Preparation

Liquid fuels contain a large number of different molecules and vary in chemical properties. A military POSF number usually classifies these fuels. Jet-A is usually classified into three types, A-1, A-2, and A-3, which are the best case, average, and worst case petroleum jet fuel, respectively. These types of jet fuel are made using different blends of distilled fuels; therefore, their average molecular formula is expected to be different. In addition, a small variation of the average chemical formula is expected for each batch of the same type of fuel. However, knowledge of the average chemical formula of the fuel is essential to prepare an accurate fuel/air mixture. Table 5 shows some properties of the three fuels used in this study along with their average chemical formula. The average chemical formula was provided by [3, 38] and it was found using a GCxGC chromatography test. These formulas were used to define fuel/air stoichiometry for each mixture (shown in Table 6).

Table 5: Properties of the three studied fuels.

Fuel	Military POSF#	Average Molecular Weight (g/mole)	Average Molecular formula	Composition by volume
Jet-A	10325	159	$C_{11.4}H_{22.1}$	18.7% Aromatics 29.5% iso-Paraffins 20.5% n-Paraffins 31.9% Cycloparaffins
RP-1	5235	168	$C_{12}H_{24.1}$	0.2% Aromatics 37.2% iso-Paraffins 0.5% n-Paraffins 62.1% Cycloparaffins
DF-2	12758	182	$C_{13.1}H_{24}$	27.6% Aromatics 23.5% iso-Paraffins 14.1% n-Paraffins 34.8% Cycloparaffins

Table 6: Molar composition of mixtures.

Fuel	ϕ	X_{fuel}	X_{O2}	X_{N2}
Jet-A	0.5	0.006168	0.208788	0.785044
	1.0	0.012260	0.207510	0.780230
RP-1	0.5	0.005794	0.208867	0.785339
	1.0	0.011521	0.207664	0.780815
DF-2	0.5	0.005470	0.208935	0.785596
	1.0	0.010879	0.207798	0.781322

To prepare the liquid fuel/air mixtures, several adjustments to the experimental setup were conducted. First, a septum injection port was installed on the mixing tank to allow direct liquid fuel injection. Also, a thermocouple was installed to measure the temperature of the mixing tank. Nevertheless, many issues, such as fuel condensation, were encountered during the development of a reliable method of preparing mixtures. The next two sub-sections go into detail on the "trail-and-error" process that was performed to reach the final mixing method procedure.

2.5.1 Mixing Tank Method

The first attempted method to prepare a liquid fuel/oxidizer mixture was using a separate heated mixing tank. This method was used in most of the previous liquid fuels studies. However, preparing mixtures using this method was challenging (discussed next) mainly due to the driven section volume of the shock tube used in this study.

In shock-tube experiments, the initial fuel/oxidizer pressure in the driven section (P_1) is directly proportional to the desired post-shock pressure (P_5). Thus, performing high-pressure experiments leads to larger (P_1), hence larger amounts of fuel. However, the amount of fuel injected is limited by the vapor pressure of the fuel. To gage the vapor pressure of each fuel, a simple experiment was conducted by injecting various amounts of liquid fuel into the mixing tank and observing the pressure. Figure 7 shows these measurements for the three fuels used in this study at a mixing tank temperature of 120°C.

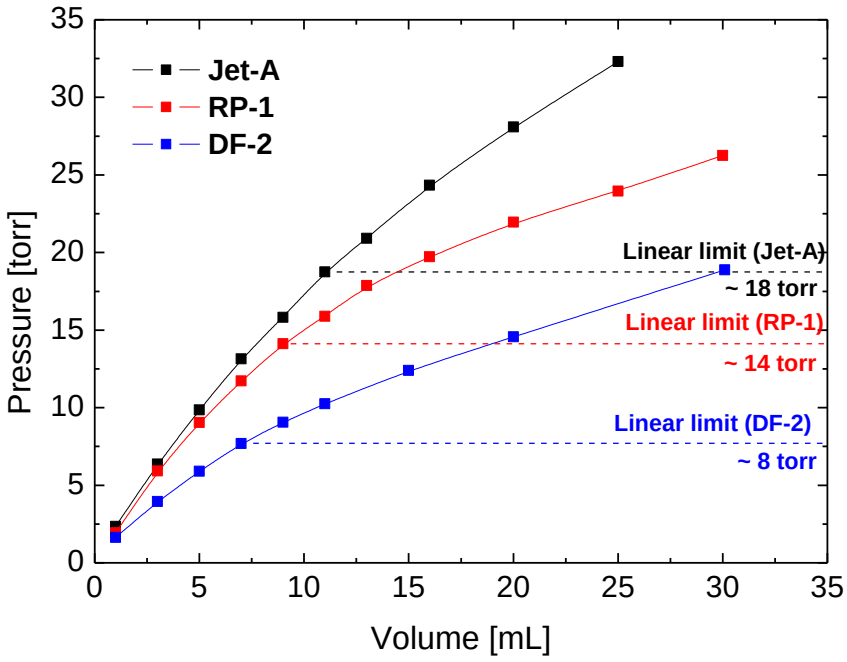

Figure 7: Liquid fuel injected volume versus pressure at a mixing tank temperature of 120 °C.

The three fuels exhibit similar behavior such that a linear region, where volume is proportional to pressure, is present at low injected volumes followed by a nonlinear region where additional fuel leads to only a slight pressure increase. This nonlinear region could be explained by the condensation of the liquid fuel heavy components. Also, the presence of cold spots in the mixing tank could cause local condensation if the local vapor pressure is reached. In any case, preparing mixtures should be constrained to the linear region to avoid condensation of the fuel, which leads to incorrect mixtures.

The maximum volume of fuel injected into the mixing tank, governed by the linear region, is shown in Figure 7 for each fuel. At these limits, preparing mixtures in the mixing tank becomes impractical for high-pressure experiments. This limitation is due to the large volume of the driven section (27.4 L). In addition, the mixing tank volume is 12 L; thus a large amount of mixture is needed to fill the driven section. For example, to perform a shock-tube experiment of post-shock conditions of 20 atm and 1000 K for a stoichiometric RP-1/air mixture, the initial driven section pressure (P_1) should be about 770 torr. To reach this amount of pressure by filling gas from the mixing tank, the pressure of the mixing tank should be around 38 psi. The amount of fuel needed to make a stoichiometric RP-1/air mixture is 22.5 torr. This pressure is well beyond the linear region of RP-1 fuel. Moreover, more challenges are expected for DF-2 fuel due to its lower vapor pressure.

As mentioned previously, several groups, such as Stanford and Rensselaer Polytechnic Institute, have been successful in testing Jet-A fuel at high pressure using the mixing tank method. This method was successful because of the smaller volume of their shock-tube driven sections, 13.3 L and 10.5 L, respectively; whereas the driven section of this study is 27.4 L. Table 7 shows a few shock-tube parameters comparison with these groups. The small volume of the driven section

allows other groups to practically perform high-pressure shock-tube experiments of Jet-A. It would be unlikely that they would be able to perform high-pressure experiments with the same methodology for RP-1 and DF-2 due to their even lower vapor-pressures. This method was able to be performed in the current study at 10 atm with Jet-A, but for all other conditions the tube mixing method, described hereafter, was necessary.

Table 7: Shock-tube driven section and mixing tank comparison with other groups.

Group	Driven section			Mixing Tank
	Diameter (cm)	Length (m)	Volume (L)	Volume (L)
Rensselaer Polytechnic	5.7	4.11	10.5	Not available
Stanford	7.5	3.0	13.3	12.8
Texas A&M	15.24	4.72	27.4	12.0

2.5.2 Tube Mixing Method

Due to the reasons explained above, another method of preparing mixtures was needed. The Duisburg group [39] has previously shown that mixtures can be made directly in the driven section without significant effect on ignition delay time measurements. However, no studies have been conducted on heavy multicomponent fuels mixtures using this method. Thus, two main issues needed to be considered as follows: ensuring that the fuel is fully vaporized after injection into the driven section and ensuring that the fuel and oxidizer are well mixed.

First, to ensure that the liquid fuel injected into the driven section is fully vaporized, various amounts of fuel were injected while observing the pressure of the driven section. The three fuels used in the present study behaved the same as follows: after injecting the liquid fuel into the evacuated driven section, the pressure fluctuates until reaching a minimum (typically after 3-5 minutes) after which the pressure increases until it stabilizes (typically after 6-8 minutes). The

increase in pressure after that was at the same rate as the incoming leaks. The stabilized pressure has been observed for 30 minutes to assure that the only increase in pressure was due to leaks. Therefore, a time period of 10 minutes was used as a standard routine to ensure that all injected fuel components are fully vaporized.

Second, to ensure that the fuel and oxidizer were well mixed, two ports along the driven section were used to fill the air mixture. This multipoint injection creates turbulence and increases mixing for a homogeneous mixture. Several ignition delay times were collected and compared to the results found in the literature to ensure that the fuel/oxidizer are well mixed (discussed later).

Figure 8 shows the first setup, denoted as “setup#1”, of the fuel injection and air filling ports. The setup is as follows: a port, located 1.6 cm from the endwall, is used to inject the liquid fuel using a septum/needle. The same port is also connected to the manifold via a PFA flexible tubing. The manifold is also connected to the driven section via another port located close to the diaphragm section. Therefore, after injecting the fuel, the air is introduced to the driven section via the manifold into the two ports.

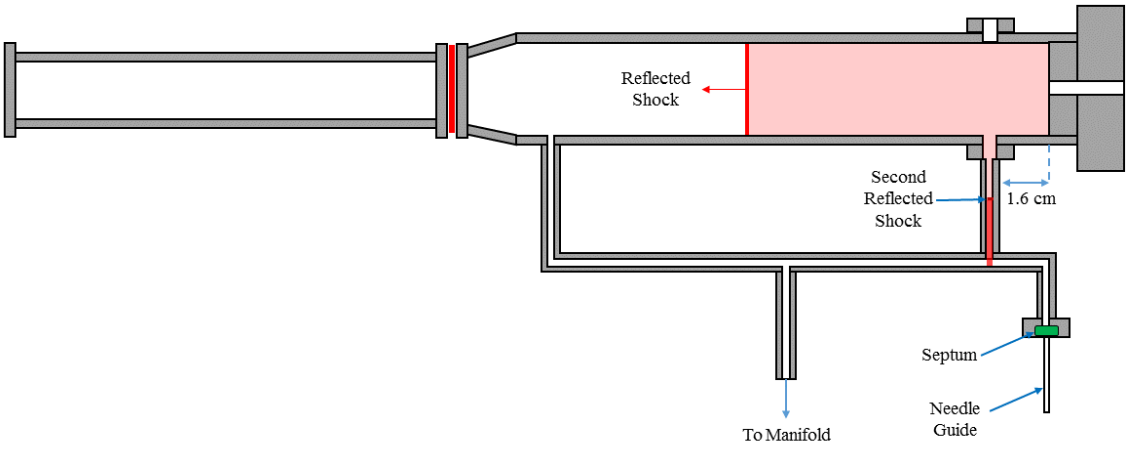

Figure 8: Schematic of "Setup#1" for making mixtures directly in the shock tube.

Several ignition delay time experiments were conducted using this setup and compared with a study by Davidson et al. [10]. Figure 9: Ignition delay time comparison of "Setup#1" with Davidson et al. for Jet-A/air at ϕ=1.0 and 10 atm. Figure 9 shows the comparison of Jet-A/air mixture at an equivalence ratio of 1.0 and a reflected shock pressure of 10 atm. Although most of the ignition delay times are within the uncertainty range of the measurements of Davidson, there is a trend of shorter ignition delay times at lower temperature. After examining the emission profiles for these measurements, no abnormal behavior was found for the high-temperature measurements (above ~1100K). However, a pre-ignition behavior was consistently observed for the lower-temperature measurements. This pre-ignition was detected at around 700-1000 µs as shown in Figure 10 and Figure 11.

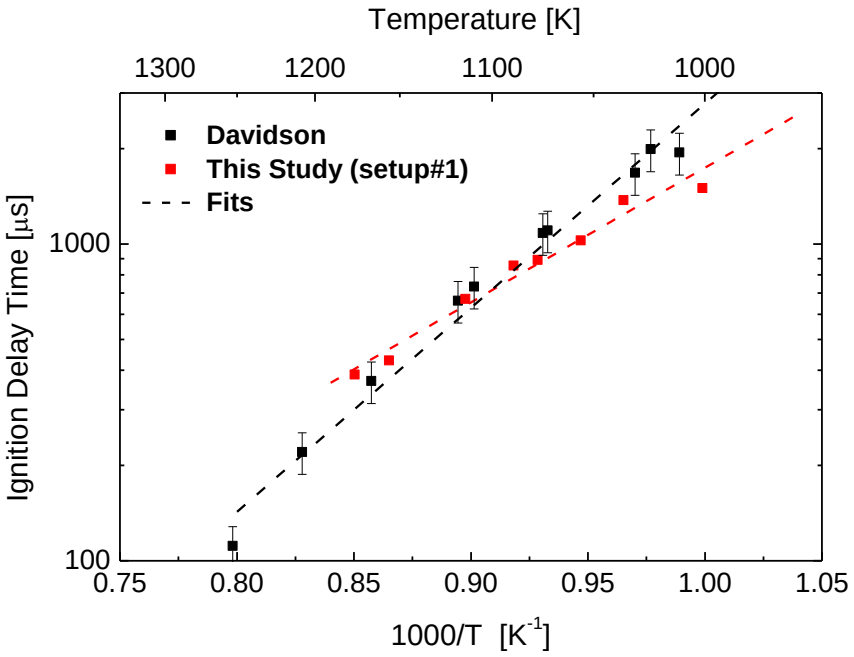

Figure 9: Ignition delay time comparison of "Setup#1" with Davidson et al. for Jet-A/air at ϕ=1.0 and 10 atm.

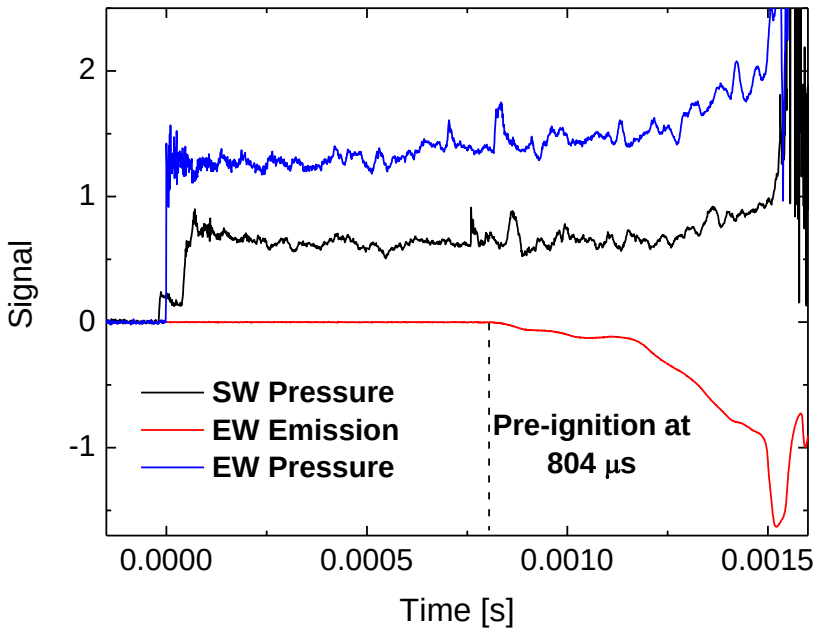

Figure 10: Ignition delay time experiment using "Setup#1" for Jet-A/air at ϕ =1.0, 1001K, and 10.3 atm

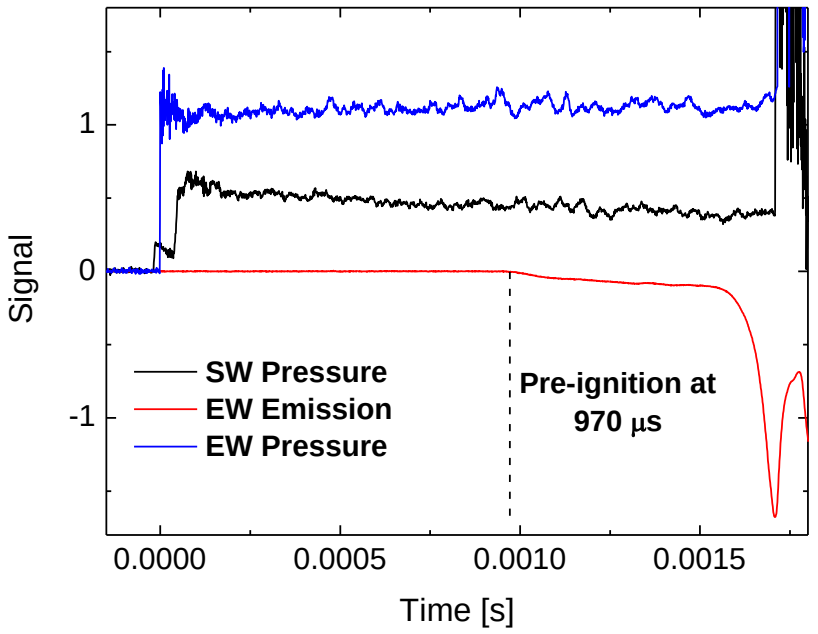

Figure 11: Ignition delay time experiment using "Setup#1" for Jet-A/air at ϕ =1.0, 1036K, and 8.4 atm

To investigate the pre-ignition behavior, a photomultiplier tube (PMT) was placed on the top port, directly viewing the filling port near the endwall as shown in Figure 12. This detector setup was done to check if there is ignition, or an emission signal, in the filling port before that main ignition at the endwall. The traces for the shock-tube experiment with this setup are shown in Figure 13. The PMT observing the filling port at the endwall captured an emission signal at ~300 µs, which is before the main ignition occurs at ~1300 µs. This emission signal can be explained by the shock traveling through the filling port and bouncing several times to create a temperature higher than the endwall temperature. Thus, the filling port higher temperature leads to faster ignition which is observed from the small emission profile at around 300 µs. This small, local ignition at the filling port increases the temperature at the endwall leading to a faster ignition delay time of the mixture.

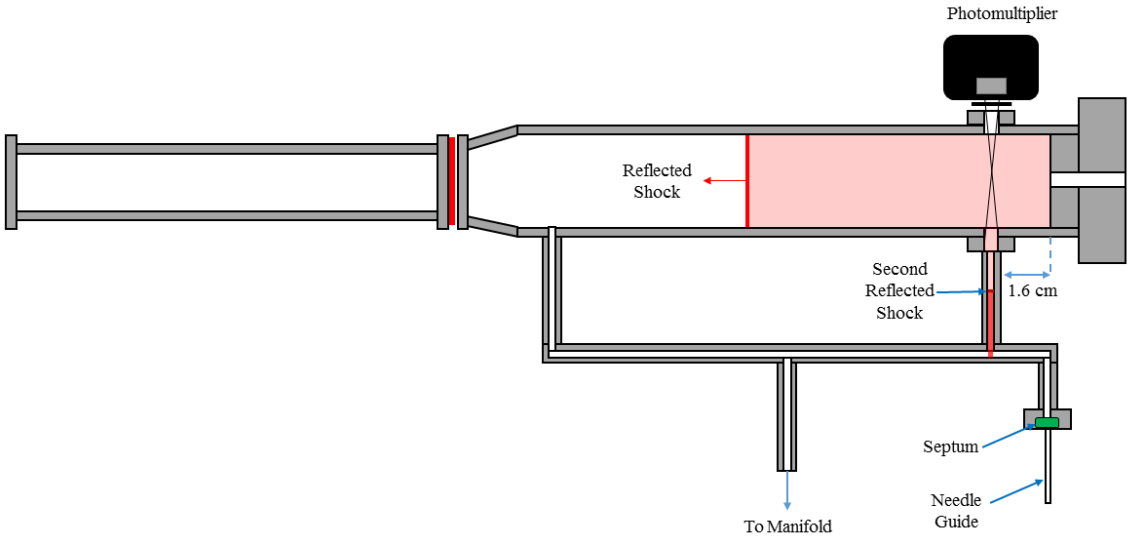

Figure 12: Schematic for setup to investigate pre-ignition behavior.

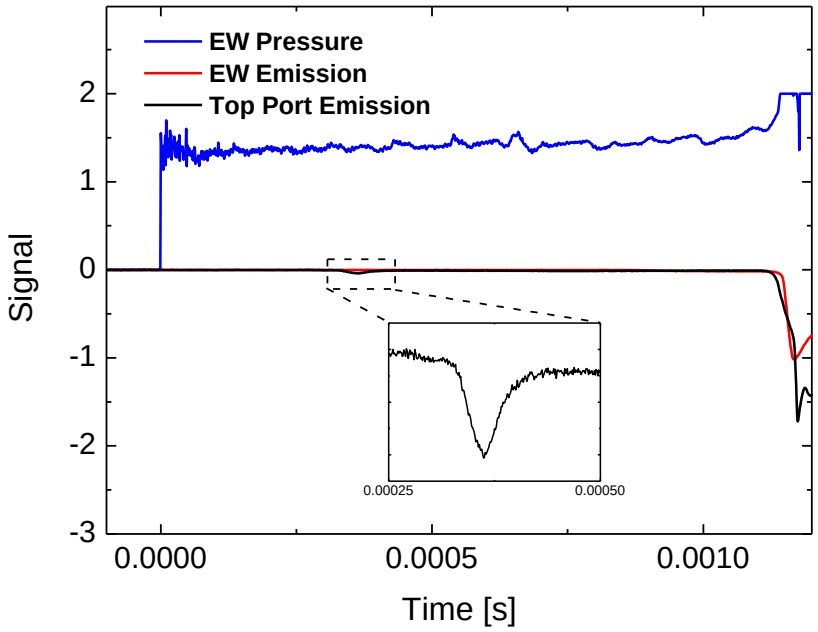

Figure 13: Ignition delay time experiment to investigate pre-ignition behavior.

To solve this pre-ignition behavior, a new setup denoted as “setup#2” was used. The setup is shown in Figure 14, where the filling port near the endwall is moved away to a location 2 m away.

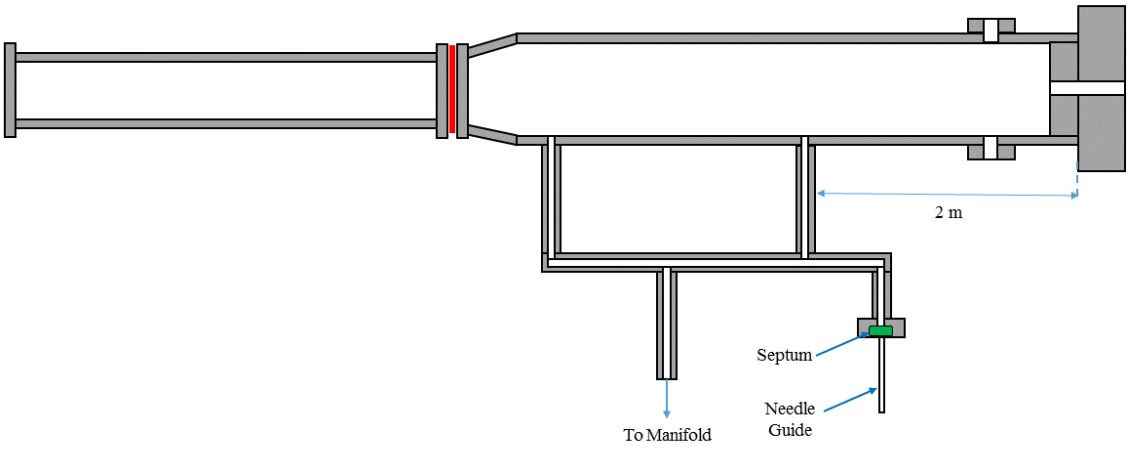

Figure 14: Schematic of "Setup#2" for making mixtures directly in the shock tube.

Moving the filling port away from the endwall was done to prevent the pre-ignition behavior occurring at the filling port. However, a concern with this setup is that the fuel and air will not be well mixed especially near the endwall region. To investigate this, several ignition delay time measurements were performed for Jet-A/air mixtures at a pressure of 10 atm and ϕ=1.0. These ignition delay times were compared with the study of Davidson et al. [10]. In addition, these measurements were compared with ignition delay time measurements obtained by making the same mixture in the mixing tank. Figure 15 shows that the ignition delay times of both mixing methods are in a very good agreement. In addition, the ignition delay times are also invery good agreement with the study of Davidson et al. Thus, this favorable comparison shows no significant influence of mixing procedure on ignition delay time. That is, preparing mixtures via "setup#2" produced suitably well-mixed conditions.

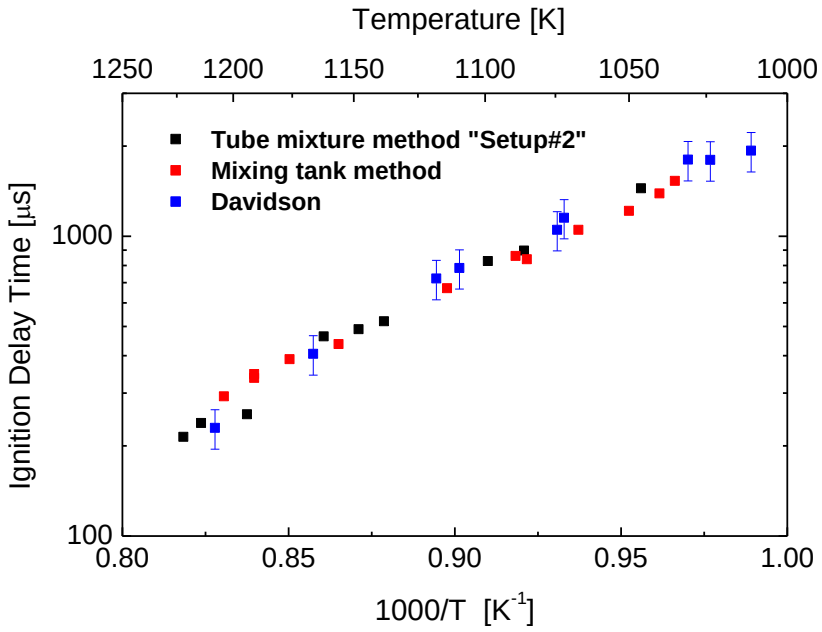

Figure 15: Comparison of ignition delay time measurements using different methods of preparing mixtures and results from [10]. Measurements for Jet-A/air at ϕ=1.0 and 10 atm (scaled using P^{-1}).

Therefore, the method used to prepare large hydrocarbons mixtures for high-pressure tests is summarized as follows:

1- The filling ports should be arranged as shown in "setup#2" to prevent local ignition near the endwall.
2- The liquid fuel is first injected via the septum injection port and left for 10 minutes to achieve full vaporization.
3- To reach the desired equivalence ratio, the fuel and air are controlled manometrically, and the amount of fuel is determined via the molar composition values given in Table 6.
4- The filling rate of air should be conducted slowly to prevent fuel condensation as discussed in [40].
5- The fuel/air mixture is then kept anywhere between 10-20 minutes to allow mixing before performing the shock experiment.
6- Leak checks must be conducted regularly when using this method of preparing mixtures.

2.6 Modeling Ignition Delay Time

In this study, the ignition delay time predictions from several kinetics mechanisms were compared with the experimental shock-tube measurements. These predictions were carried out using a closed, homogenous batch reactor via CHEMKIN 19.0 by constraining the volume and solving the energy equation. None of the kinetics mechanisms accounted for OH* reactions; therefore, the mechanism of Hall and Petersen [41] was added to allow prediction of OH* time histories. Ignition delay time predictions were obtained by extrapolating the steepest slope of OH* from the model simulation to zero.

CHAPTER III

RESULTS AND DISCUSSIONS

This chapter describes ignition delay time measurements for several fuels. First, n-alkane ignition delay times were investigated to create a baseline and to compare the results with measurements of other groups. Then, ignition delay times are presented for the three multicomponent liquid fuels under investigation in this study. Next, a comparison of experimental results with previously published data from the literature is presented, followed by high-temperature correlations for each fuel. Finally, a comparison with several chemical kinetics mechanisms is presented. All of the experiment data are presented in Appendix A.

3.1 n-Alkanes Ignition Times

To validate the ignition delay time using the new heated facility, several baseline ignition delay time experiments were conducted for four n-Alkanes fuels. These fuels were selected based on the available, previously published data from other groups to allow direct comparison.

3.1.1 n-Pentane

Ignition delay times for stoichiometric n-Pentane and 4% O_2 diluted in argon were measured behind a reflected shock wave at a pressure around 2 atm for a temperature range of 1261-1508 K. Measurements of ignition delay times for the same fuel under the same conditions had been performed previously by Davidson et al. [42]. Figure 16 shows a comparison between the two sets of ignition delay times. All of the ignition delay times have been scaled to a pressure of 2 atm using a factor of 0.52, which was suggested in the study of Davidson. After scaling, the current study's ignition delay times are in excellent agreement with Davidson's data.

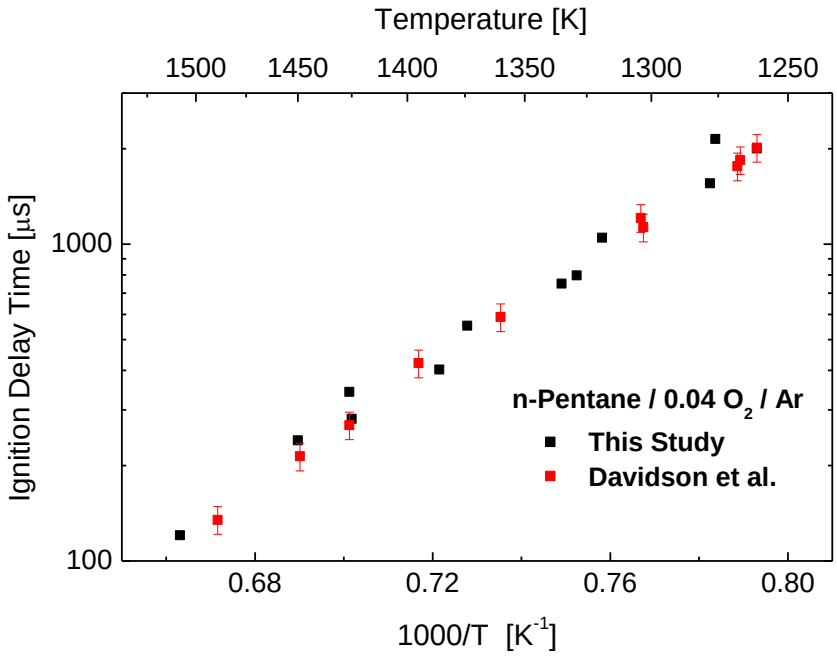

Figure 16: Ignition delay time comparison with Davidson et al. [42] for n-C5H12/4%O_2/Ar at ϕ=1.0 and 2 atm.

3.1.2 n-Octane

Ignition delay times for stoichiometric n-octane and 4% O_2 diluted in argon were measured at a pressure around 2 atm and a temperature range of 1280-1440 K. The shock-tube temperature was set to 90°C. Direct comparison with Davidson et al. [42] is presented in Figure 17. The two sets of data are in a very good agreement. All the ignition delay times were scaled to 2 atm using a pressure factor of 0.52.

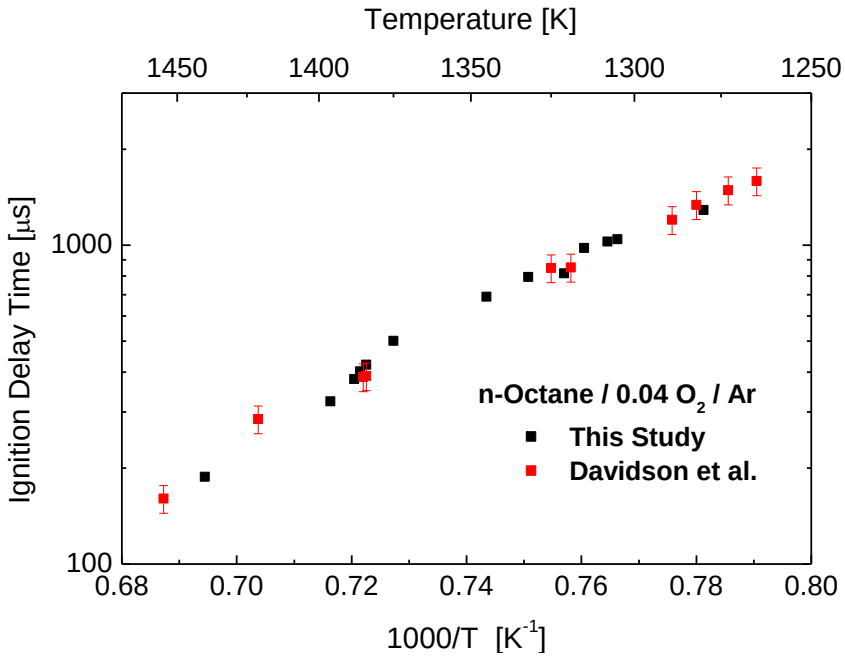

Figure 17: Ignition delay time comparison with Davidson et al. [42] for n-C_8H_{18}/4%O_2/Ar at ϕ=1.0 and 2 atm.

3.1.3 n-Nonane

Ignition delay times for n-nonane and 4% O_2 diluted in argon at an equivalence ratio of 1.0 are shown in Figure 18. The measurements are scaled to 2.0 atm and are compared with the results of two previous studies. Davidson et al. [42] measured ignition delay time using endwall emission, while He et al. [43] used sidewall emission. There is a good agreement between both studies, and no effect of emission diagnostics setup was evident. However, the ignition delay times from this study predicts a slightly longer times.

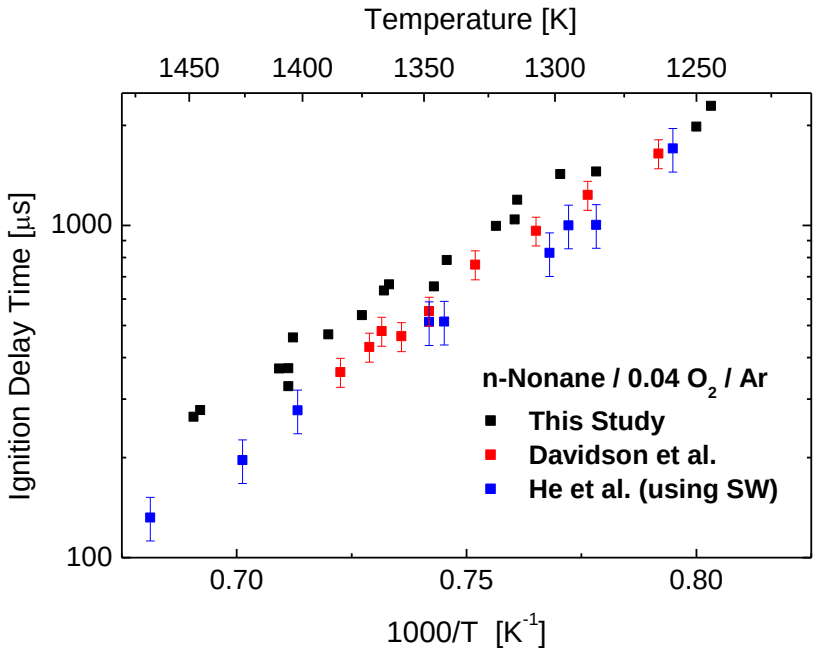

Figure 18: Ignition delay time comparison with Davidson et al. [39] and He et al. [43] for n-C_9H_{20}/4%O2/Ar at ϕ=1.0 and 2 atm.

To investigate this difference, several ignition delay time measurements were conducted using different methods. One of the concerns is that the fuel, n-nonane, was sticking to the inside wall of the tube creating a fuel rich mixture which leads to longer ignition delay times for these highly diluted mixtures. As mentioned in the experimental setup section, a turbomolecular pump is used to vacuum the driven section prior to introducing the fuel/oxidizer mixture. Typically, 7-10 minutes of vacuuming are sufficient to reach a pressure of ~1×10^{-5} torr. However, no investigations have been conducted on vacuum efficiency while using heavy liquid fuels.

Since the initial n-nonane ignition delay time measurements were different from those of the previous studies, several methods were used to measure ignition delay time. This comparison was performed to confirm the accuracy of the earlier measurements. First, the vacuuming times were varied to investigate the possible fuel leftover in the driven section and study the effect on

ignition delay time. Second, argon shocks were performed prior to the n-nonane experiments. Finally, the tube was physically cleaned prior to performing each n-nonane ignition delay time experiment. Figure 19 shows ignition delay time measurements collected using different methods and compared with those of Davidson et al. [42]. The results show consistently longer ignition delay time for all cases.

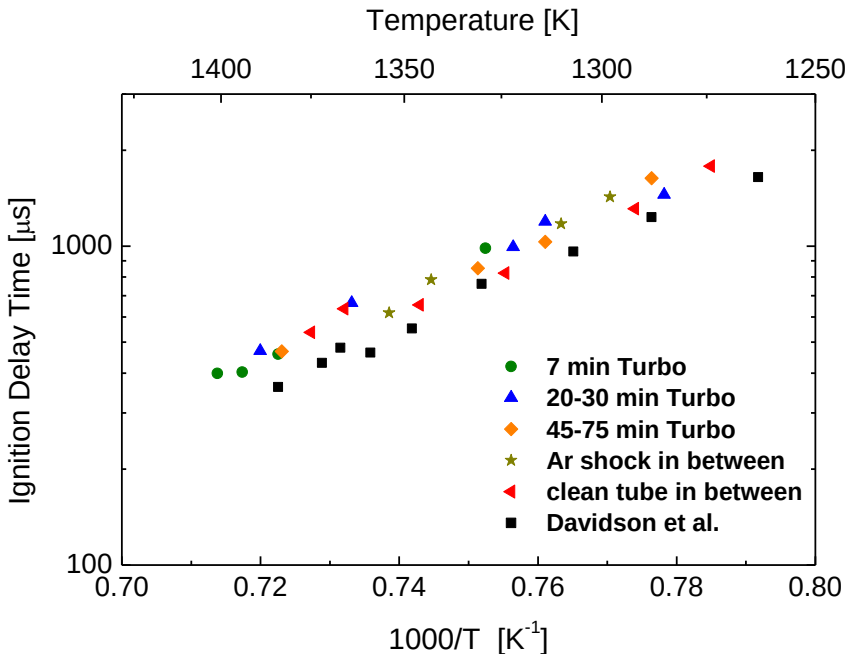

Figure 19: Ignition delay time measurements using different methods for n-C_9H_{20}/4%O_2/Ar at ϕ=1.0 and 2 atm.

3.2 Jet Fuel Ignition Delay Time

The ignition delay time for Jet-A/air at equivalence ratios of 0.5 and 1.0; pressures of 10 atm and 20 atm; and a wide range of temperatures is shown in Figure 20. At 10 atm, equivalence ratio appears to have no effect on ignition delay time for high temperatures (above ~1150 K), while slight differences in ignition are present at lower temperatures with the fuel lean case showing longer ignition delay times. At 20 atm, the equivalence ratio effect is evident with the

stoichiometric condition showing shorter ignition delay times. At ϕ = 0.5, ignition delay time increases with decreasing temperature for the high-temperature region (above ~950 K), and negative-temperature-coefficient (NTC) behavior is evident at temperatures lower than 900 K.

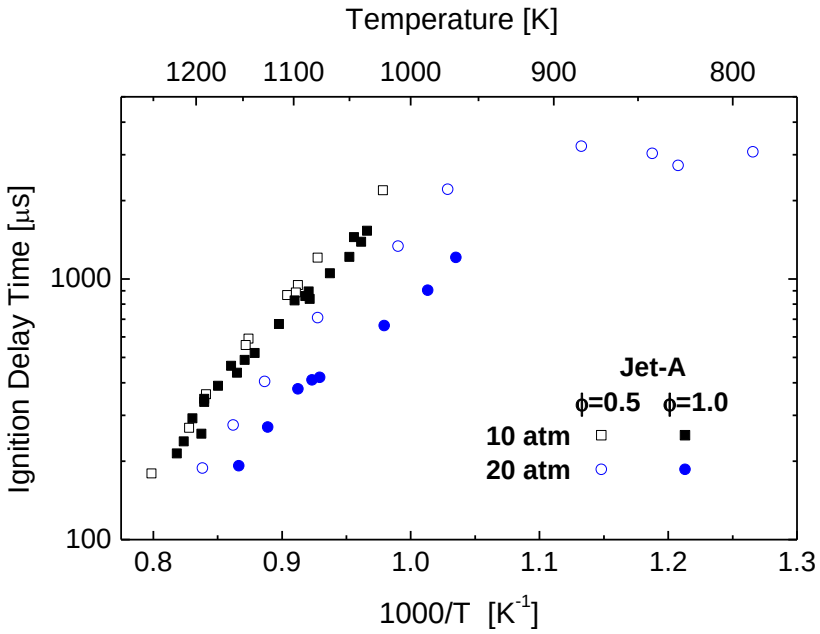

Figure 20: Ignition delay time measurements for Jet-A/air at ϕ=0.5 and 1.0, and a pressure of 10 and 20 atm (scaled using factor provided in Table 8).

As mentioned previously, several studies have been reported on the ignition delay time of Jet-A. However, several blends of jet fuel, usually classified by military POSF number, have been used in these studies. Davidson et al. [10] and Burden et al. [12] tested Jet-A (POSF 10325), which is the same blend of Jet-A used in this study. Davidson et al. measured ignition delay times for the same mixture in an aerosol shock tube at a pressure of 10 atm, while Burden et al. used a heated shock tube to collect ignition delay times at a pressure of 20 atm. There is very good agreement among ignition delay times from this study with other measurements of the same fuel blend. Figure 21 shows a comparison of these measurements for Jet-A in air at an equivalence ratio of 1.0 at two

pressures, 10 and 20 atm, and over a wide range of temperature. All the ignition delay times have been scaled using P^{-a}, where a is the pressure coefficient in Table 8 (discussed later). A representation of the uncertainty in the ignition delay times is shown for selected points at a wide range of temperature.

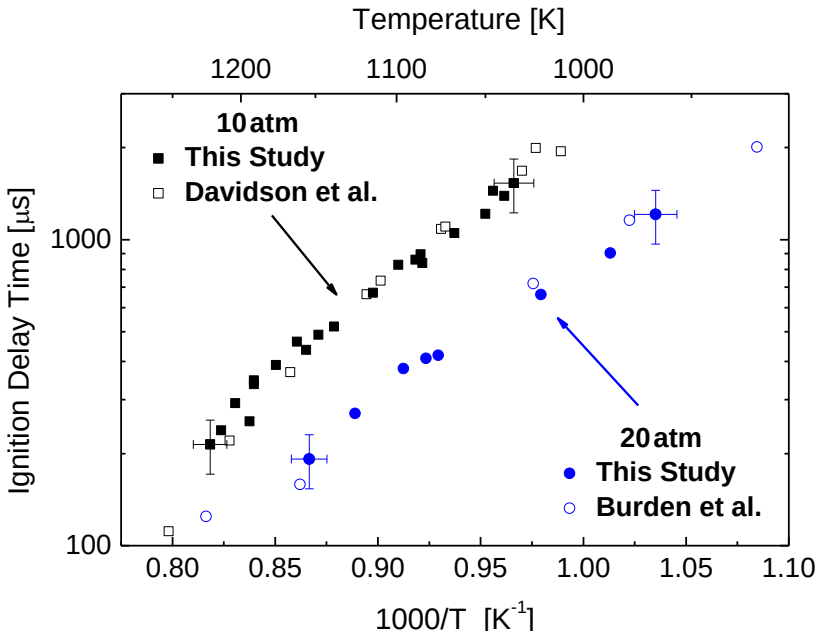

Figure 21: Comparison of ignition delay times of Jet-A/air at ϕ=1.0 with Davidson et al. [10] and Burden et al. [12].

Jet-A, JP-8, and JP-5 are the three main types of jet fuels. However, each type has subtypes which are classified by the military POSF number. Wang et al. [8] measured ignition delay time for a different blend of Jet-A, POSF 4658, at a pressure of 10 atm. This fuel was prepared in the Air Force Research Laboratory, and it is a composite of approximately five, equal amounts of Jet-A batches from different manufacturers [44]. Figure 22 shows an ignition delay time comparison between Wang's results and this study. There is a considerable difference between the ignition

delay times of the two different blends, with the POSF 4658 blend showing shorter ignition delay times. However, at lower temperatures, this difference tends to decrease.

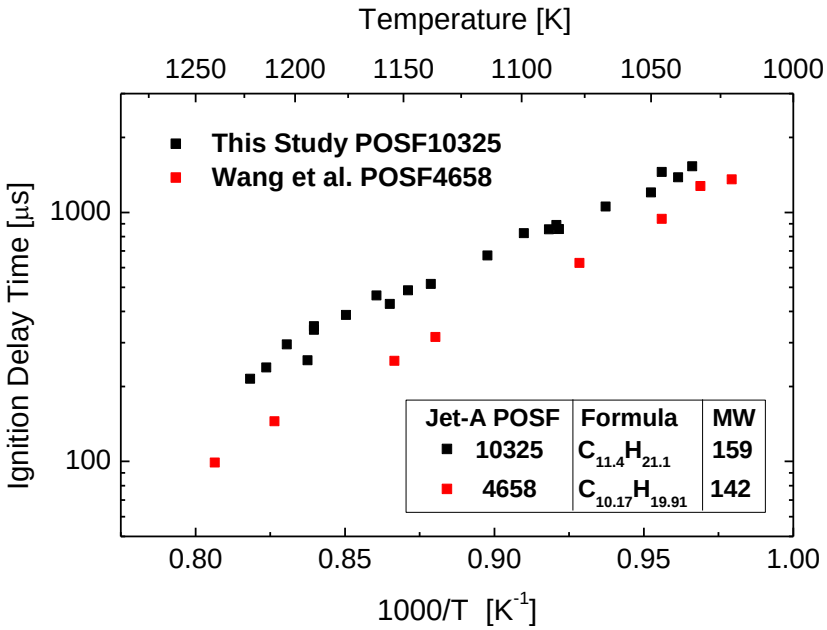

Figure 22: Ignition delay time comparison with Wang et al for different blends of Jet-A in air at 10 atm and ϕ=1.0.

Several earlier studies investigated the ignition delay time of different types of jet fuels such as JP-8 and JP-5. Davidson et al. [10] measured ignition delay times for both JP-8 and JP-5 in air using an aerosol shock tube at a pressure of around 10 atm and an equivalence ratio of 0.85-1.15. To allow a direct comparison, pressure and equivalence ratio scaling factors were used. The pressure scaling factor (-1.194) provided in the Davidson et al. study was utilized. However, Davidson did not provide an equivalence ratio factor, and the factor from the analysis of the present study was utilized (discussed later in this thesis).

Moreover, Vasu et al. [6] and Burden et al. [12] studied the ignition delay times of JP-8 and JP-5 at a pressure of 20 atm using a heated shock tube. The ignition delay times from both studies were scaled using a simple P^{-1} relation. Figure 23 shows a comparison of the ignition

delay time at two pressures of 10 and 20 atm, and an equivalence ratio of 1.0. The ignition delay times are indistinguishable from each other at both pressures.

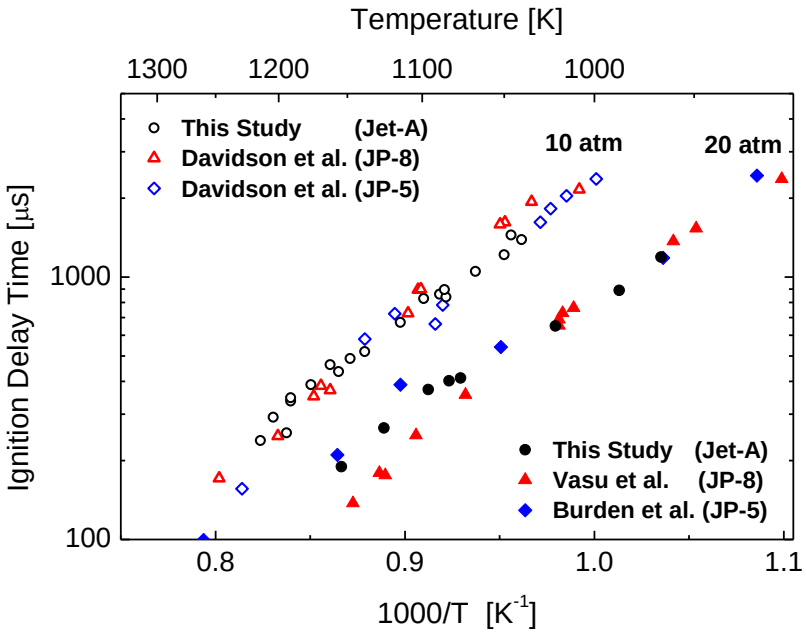

Figure 23: Ignition delay time comparison of different jet fuels in air at an equivalence ratio of 1.0 and at 10 atm (open symbols) and 20 atm (closed symbols) [6, 10, 12].

3.3 Rocket Fuel Ignition Delay Time

The ignition delay times for RP-1/air at equivalence ratios of 0.5 and 1.0; a pressure of 10 atm and 20 atm; and a wide range of temperature is shown in Figure 24. These ignition delay times of RP-1 fuel show similar behavior to Jet-A fuel. The effect of equivalence ratio is negligible at a pressure of 10 atm, while a considerable difference is observed for the 20-atm case with the stoichiometric condition showing shorter ignition delay times. At 20 atm and ϕ=0.5, negative-temperature-coefficient (NTC) behavior is evident at temperatures lower than 900 K.

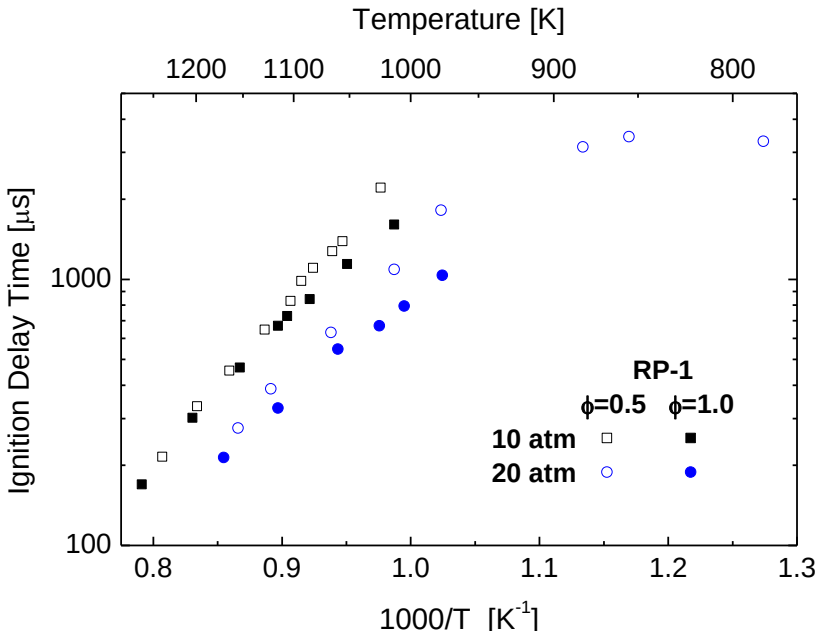

Figure 24: Ignition delay time measurements for RP-1/air at ϕ=0.5 and 1.0, and a pressure of 10 and 20 atm (scaled using factor provided in Table 8).

There are only few ignition delay time studies for rocket fuels. Davidson et al. [17] used an aerosol shock tube to measure the ignition delay times of two different blends of rocket fuel (RP-2). These blends are POSF 7688 and POSF 5433 which have an average molecular weight of $C_{12.0}H_{24.1}$ and $C_{12.6}H_{25.6}$ respectively. The measurements were conducted over a wide range of temperature and at a pressure of ~13 atm. A simple pressure factor of P^{-1} was used to scale the ignition delay times to 10 atm to allow direct comparison. Figure 25 shows that the difference in ignition delay times of RP-1 and RP-2 is insignificant.

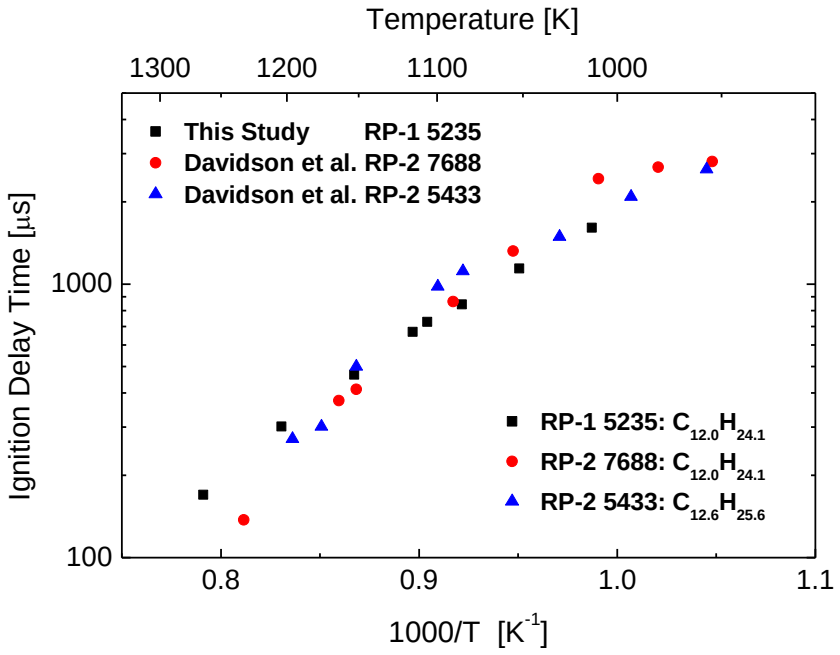

Figure 25: Ignition delay time comparison of different rocket fuel types in air at an equivalence ratio of 1.0 and a pressure of 10 atm [17].

3.4 Diesel Fuel Ignition Delay Time

The ignition delay times for DF-2/air at equivalence ratios of 0.5 and 1.0; pressures of 10 atm and 20 atm; and a wide range of temperature are shown in Figure 26. Ignition delay times of diesel fuel follow the same behavior of Jet-A and RP-1. At 10 atm, the effect of equivalence ratio is minimal at higher temperatures (above 1150 K). Small differences are noticed at lower temperatures where the fuel lean case is showing longer ignition delay times. At 20 atm, the effect of equivalence ratio is noticeable with the stoichiometric case showing shorter ignition delay times. At 20 atm and ϕ=0.5, the ignition delay time measurements extend to reach the negative-temperature-coefficient (NTC) at temperatures below 900 K.

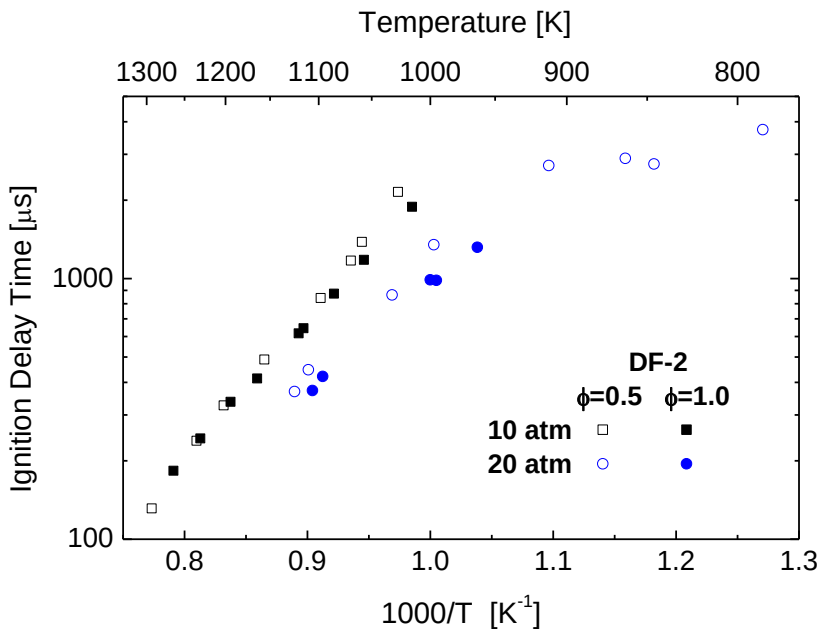

Figure 26: Ignition delay time measurements for DF-2/air at ϕ=0.5 and 1.0, and a pressure of 10 and 20 atm (scaled using factor provided in Table 8).

There are several ignition delay time studies for DF-2. However, only a few studies have been conducted using shock tubes for high-temperature combustion. Haylett et al. [26] measured ignition delay times of an unknown blend of DF-2 using an aerosol shock tube at a pressure of around 7 atm and an equivalence ratio close to 0.5. The ignition delay times have been scaled to 10 atm using the pressure factor (-0.82) provided in Haylett study. In addition, Haylett provided an equivalence ratio scaling factor of (-0.7) which was used to scale the data to an equivalence ratio of 0.5. This adjustment allows direct comparison as shown in Figure 27. The ignition delay times are in reasonable agreement for the low-temperature region (below ~1150 K). However, there is considerable scatter in the ignition delay times reported by Haylett at higher temperatures.

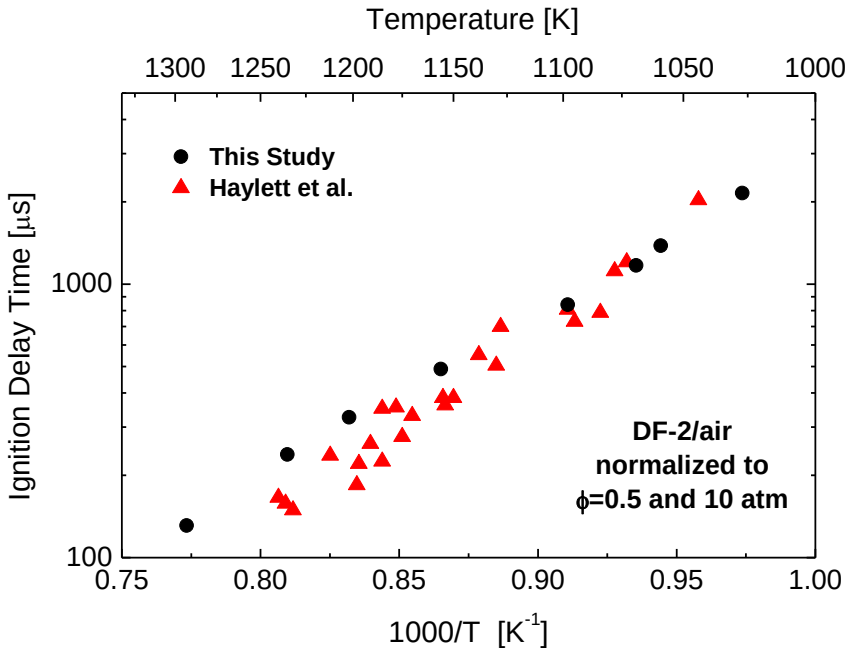

Figure 27: Ignition delay time comparison for DF-2 in air with Haylett et al. [26] at a pressure of 10 atm and an equivalence ratio of 0.5.

Moreover, Davidson et al. [10] used an aerosol shock tube to measure ignition delay times for a different blend of DF-2 (POSF 12407) at a pressure of ~10 atm and an equivalence ratio close to 1.0. This blend has an average chemical formula of $C_{13.6}H_{25.9}$, while the DF-2 used in the present study (POSF 12758) has an average chemical formula of $C_{13.1}H_{24.0}$. Davidson provided a pressure scaling factor of (-1.194) which was used to scale the data to 10 atm. Figure 28 shows a comparison between the two blends of DF-2 in air at a pressure of 10 atm and an equivalence ratio of 1.0. There is a good agreement in ignition delay times among temperatures below 1200 K. At higher temperature, diesel fuel POSF 12407 is showing shorter ignition delay times. However, only one ignition delay time point was reported in that region, and further data are required to confirm this observation.

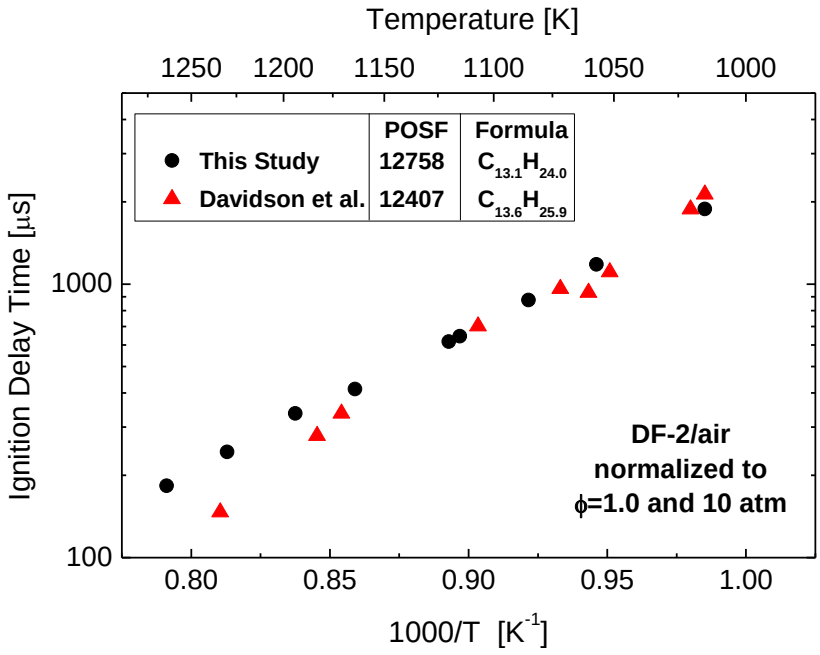

Figure 28: Ignition delay time comparison for DF-2 in air with Davidson et al. [10] at a pressure of 10 atm and an equivalence ratio of 1.0.

As mentioned earlier, the other main type of diesel fuel is the military diesel fuel F-76. Few studies investigated the ignition delay time of this type of fuel. Gowdagiri et al. [28] measured ignition delay times of F-76 in air at equivalence ratios of 0.5 and 1.0 and pressures of 10 and 20 atm. The ignition delay times have been scaled using a simple pressure factor of P^{-1} to allow direct comparison with the current study. Figure 29 compares the ignition delay times at an equivalence ratio of 1.0 and two pressures of 10 and 20 atm. There is a noticeable difference in ignition delay times, with the military diesel fuel F-76 showing shorter ignition delay times at both pressures. In addition, Figure 30 shows a comparison for a wider range of temperature, including the NTC region, at a pressure of 20 atm and an equivalence ratio of 0.5. At this condition, the military diesel fuel F-76 shows slightly shorter ignition delay times than that of DF-2.

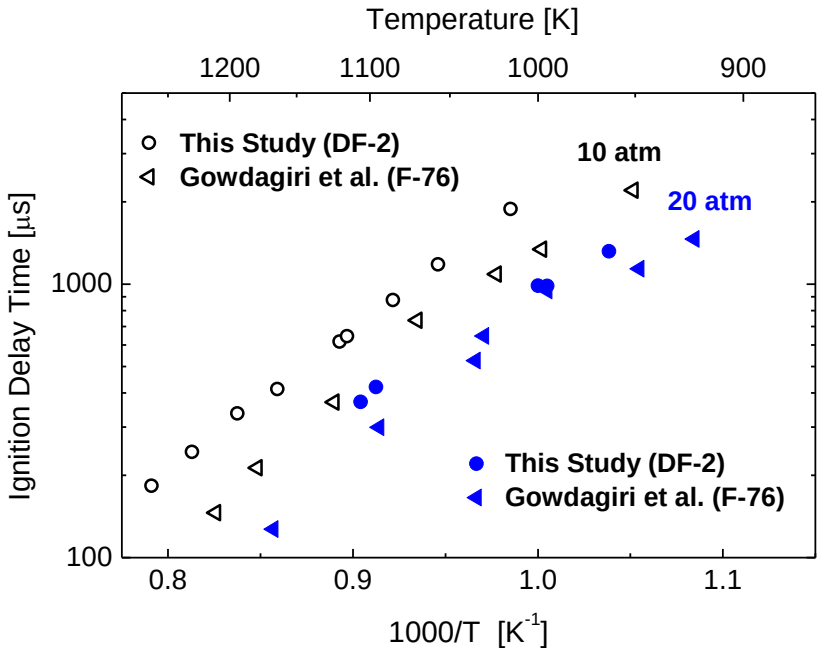

Figure 29: Ignition delay time comparison of DF-2 and military diesel fuel (F-76) in air at a pressure of 10 and 20 atm and an equivalence ratio of 1.0 [28].

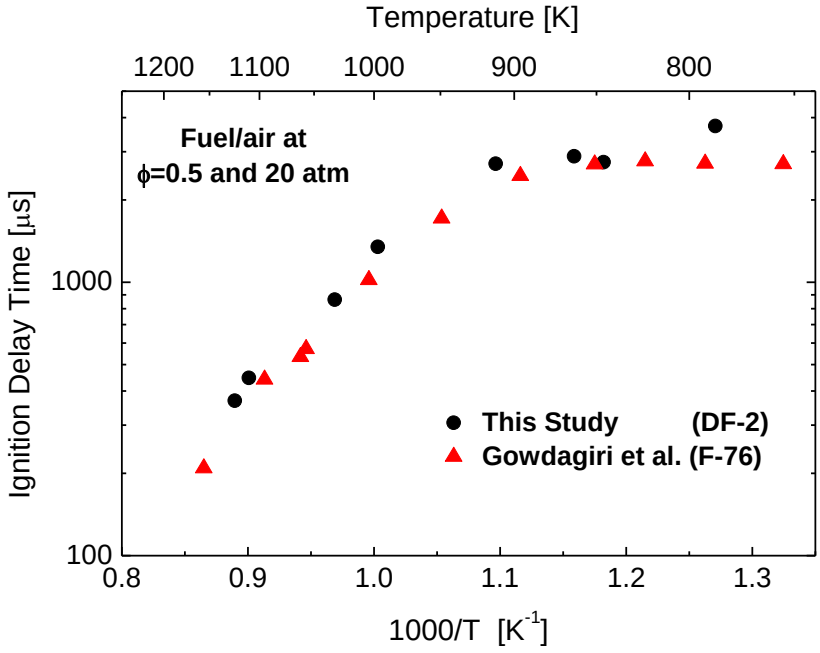

Figure 30: Ignition delay time comparison of DF-2 and military diesel fuel (F-76) in air at a pressure of 20 atm and an equivalence ratio of 0.5 [28].

3.5 Ignition Delay Time Comparison

Ignition delay times for Jet-A, RP-1, and DF-2 were collected for two equivalence ratios of 0.5 and 1.0, and two pressures of 10 and 20 atm. Figure 31 shows a comparison of the ignition delay times of the three fuels in air at a pressure of 10 atm and equivalence ratios of 0.5 and 1.0. At both equivalence ratios, the ignition delay times are indistinguishable..

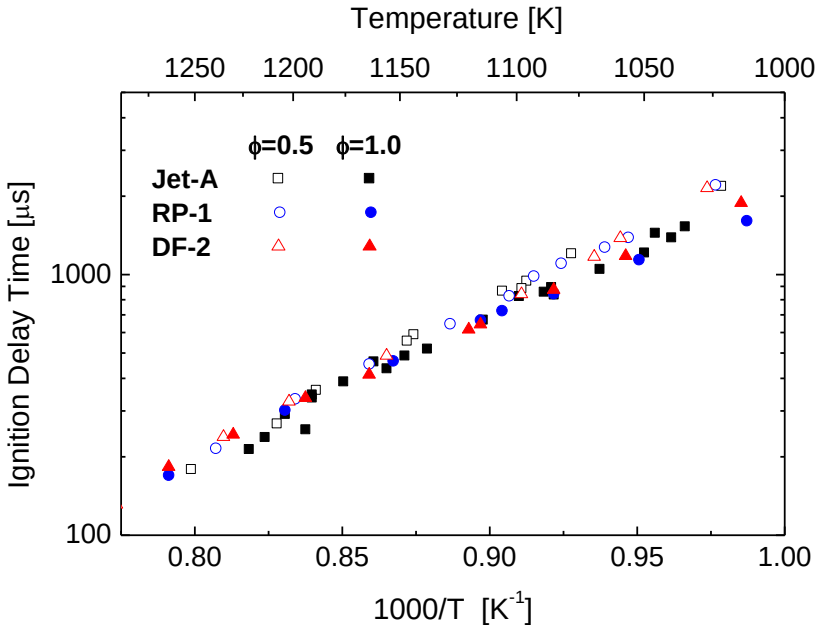

Figure 31: Ignition delay time comparison of Jet-A, RP-1, and DF-2 in air at a pressure of 10 atm and an equivalence ratio of 0.5 and 1.0.

Moreover, Figure 32 shows a comparison of the ignition delay times of the three fuels in air at a pressure of 20 atm and equivalence ratios of 0.5 and 1.0. Similar to the low-pressure case, the ignition delay times for all three fuels are in close agreement. At the NTC region, the ignition delay times show slight differences, however, more data points are needed to define the behavior in that region.

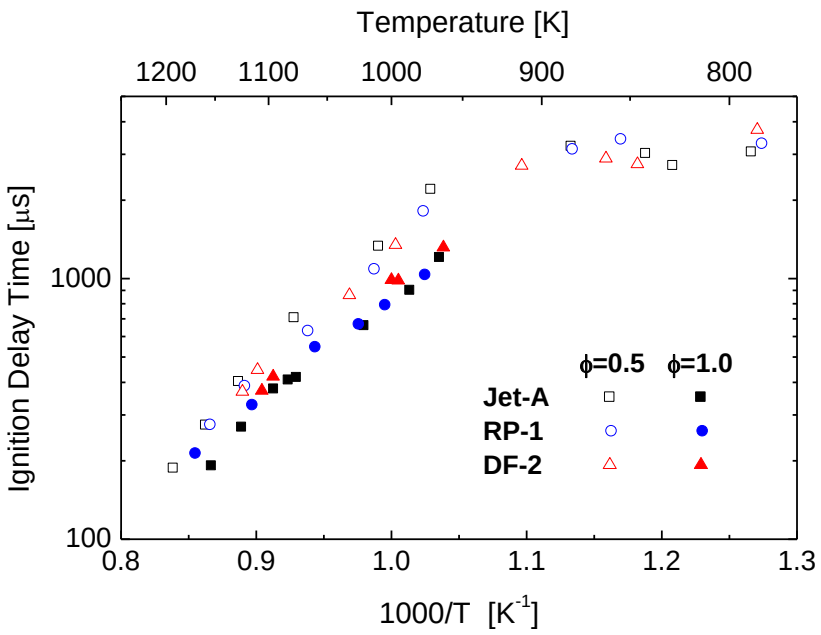

Figure 32: Ignition delay time comparison of Jet-A, RP-1, and DF-2 in air at a pressure of 20 atm and an equivalence ratio of 0.5 and 1.0.

3.6 Ignition Delay Time Correlations

Multiple linear regression analysis is utilized to develop correlations to predict ignition delay times at the higher-temperature "linear" region for each fuel. The linear regression of three independent variables (logarithmic of the pressure, logarithmic of the equivalence ratio, and the inverse of temperature) versus the dependent variable (logarithmic of the ignition delay time) was used to determine a correlation for each fuel. The effect of all three independent variables was equally weighted.

All the three fuels, Jet-A, RP-1, and DF-2, could be correlated for higher-temperature ignition above (~950 K) using an Arrhenius expression of the form

$$\tau_{\text{ign}} = A\,[P]^{-B}\,[\phi]^{-C} exp\left(\frac{E}{RT}\right) \qquad (1)$$

where τ_{ign} is the ignition delay time in μs, P is the pressure in atm, E is the activation energy in kcal/mol, T is the temperature in K, and R is the universal gas constant (1.987×10^{-3} kcal/mol-K). The mean activation energy E, the coefficients A, B, and C, and the standard error for each fuel are given in Table 8. These correlations cover a range of temperature of 950-1400 K, a pressure range of 10-20 atm, and an equivalence ratio range of 0.5-1.0. The correlations are plotted against high-temperature ignition delay times at 10 and 20 atm and ϕ=0.5 and 1.0 for each fuel.

Table 8: Constants and standard errors for ignition delay time correlations (Eqn. 1).

Fuel	A	B	C	E	Standard Error
Jet-A	0.123	1.078	0.365	24.41	13%
RP-1	0.206	0.996	0.335	22.78	11%
DF-2	0.217	0.959	0.183	22.57	13%

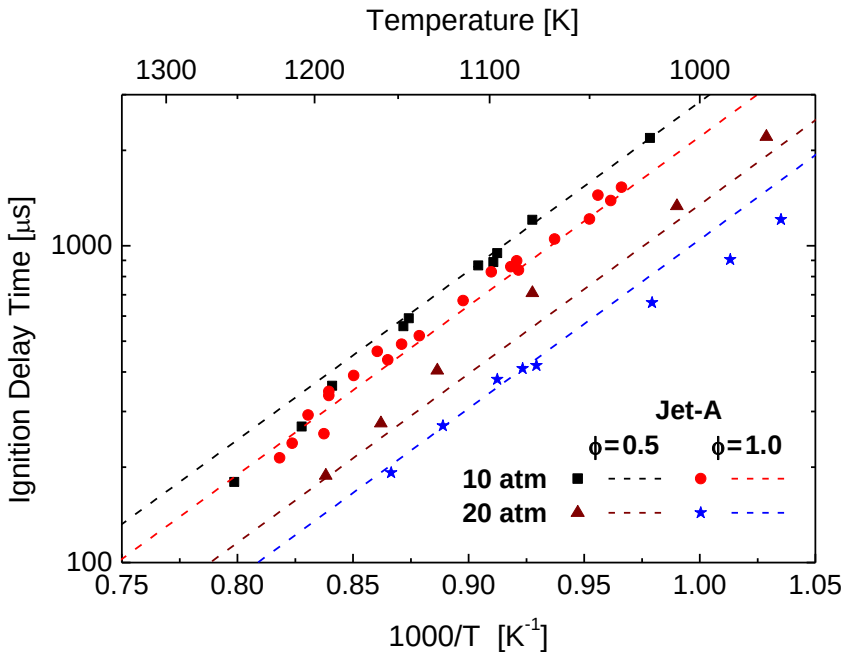

Figure 33: Ignition delay time measurements (symbols) and correlations (dotted lines) for Jet-A at pressures of 10 and 20 atm and equivalence ratios of 0.5 and 1.0.

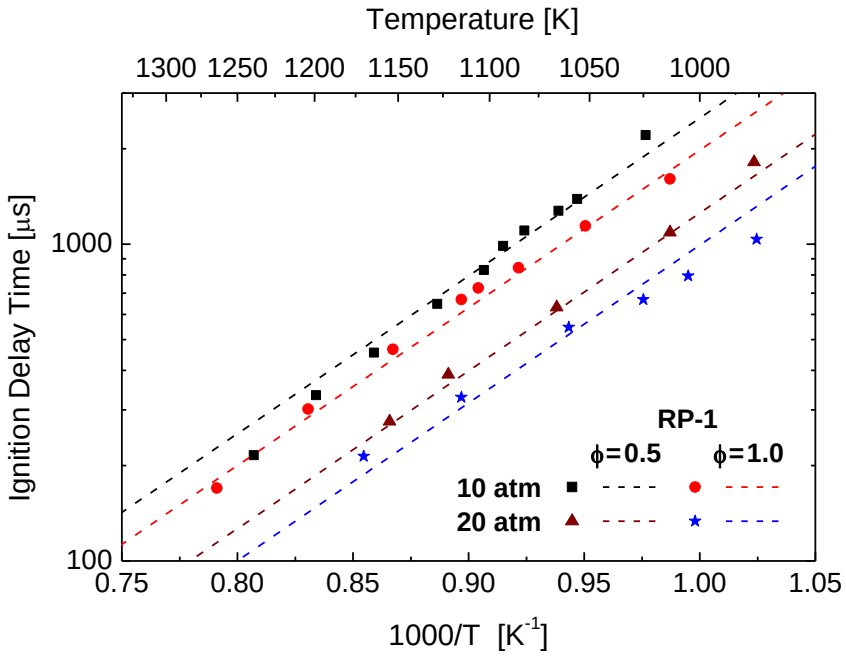

Figure 34: Ignition delay time measurements (symbols) and correlations (dotted lines) for RP-1 at pressures of 10 and 20 atm and equivalence ratios of 0.5 and 1.0.

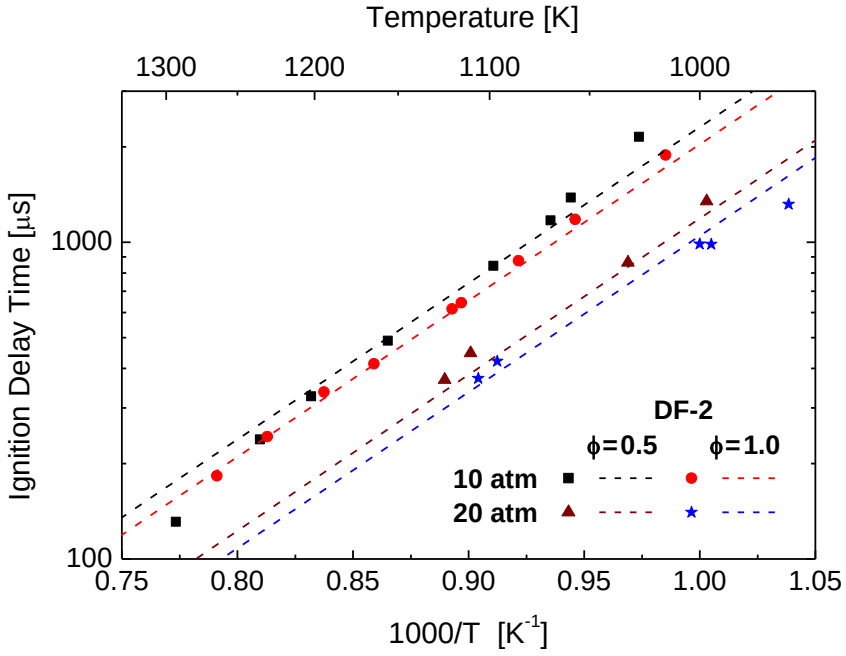

Figure 35: Ignition delay time measurements (symbols) and correlations (dotted lines) for DF-2 at pressures of 10 and 20 atm and equivalence ratios of 0.5 and 1.0.

3.7 Chemical Kinetics Mechanism Comparison

The ignition delay times obtained in this study provide validation targets for kinetics mechanisms of liquid fuels. Several groups have been active in developing kinetics mechanisms and surrogate models for jet and diesel fuels. However, there is a lack of kinetics mechanisms specifically assembled for rocket fuels. In this study, the predictions from six kinetics mechanisms for kerosene-based fuels are considered. Table 9 shows these kinetics mechanisms along with the surrogate composition used to represent the real fuel.

Table 9: Kinetic models and surrogate mixture compositions [35, 45-49].

Target Fuel	Kinetics Mechanism	Surrogate Composition (mol%)	Details
Jet Fuel	Honnet et al.(1)	77.17% n-decane 22.83% 1,2,4-trimethylbenzene	122 species 900 reactions
Jet Fuel	Malewicki et al.(2)	40.41% n-dodecane 29.48% iso-octane 22.83% n-propylbenzene 7.28% 1,3,5-trimethylbezene	2080 species 8310 reactions
Jet Fuel	Narayanaswamy et al.(3)	30.3% n-dodecane 48.5% methylcyclohexane 21.2% m-xylene	369 species 2691 reactions
Diesel Fuel	Pei et al.(6)	77% of n-dodecane 23% m-xylene	163 species 887 reactions
Diesel Fuel	Frassoldati et al.(5)	63.1% n-decane 36.9% Methyl-naphthelene	123 species 1017 reactions
Diesel Fuel	Yao et al.(4)	100% n-dodecane	54 species 269 reactions

(1) Institute for Combustion Technology, RWTH Aachen University, Germany
(2) University of Illinois at Chicago, USA
(3) Indian Institute of Technology Madras, India
(4) Lawrence Livermore National Laboratory, United States
(5) The CRECK Modeling Group, Polytechnic University of Milan, Italy
(6) Tsinghua University, China

3.7.1 Jet Fuel Mechanisms

Honnet et al. [45] from the Institute for Combustion Technology (RWTH Aachen University, Germany) developed a surrogate for kerosene-based fuels along with a kinetics mechanism. A surrogate mixture containing 80% n-decane and 20% 1,2,4-trimethylbenzene by weight was selected to represent jet fuels, particularly Jet-A, Jet-A1, and JP-8. The chemical kinetics mechanism contains 122 species and 900 reactions, and it was assembled based on two separate mechanisms for n-decane and 1,2,4-trimethylbenzene. Figure 36 shows the ignition delay time prediction from this mechanism along with the experimental results for Jet-A in air at 10 and 20 atm, and an equivalence ratio of 0.5 and 1.0. The mechanism shows satisfactory prediction of the ignition delay time at 20 atm and captures the negative-temperature-coefficient (NTC) region within the uncertainty of the experimental measurements. However, at 10 atm, it under predicts the ignition delay time for the high-temperature region.

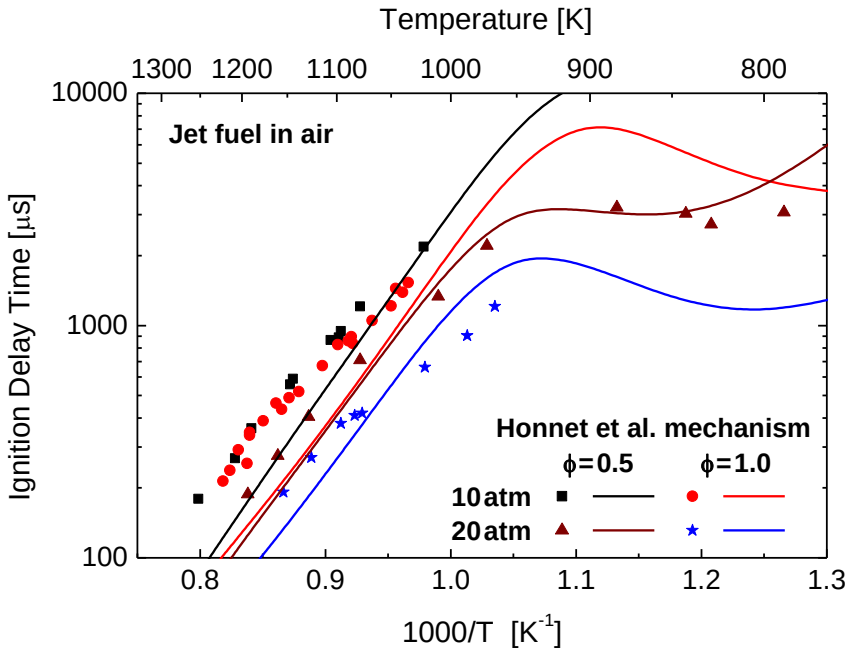

Figure 36: Prediction from the Honnet et al. mechanism for jet fuel in air for 10 and 20 atm, and ϕ = 0.5 and 1.0 [45].

Malewicki et al. [47] from the Brezinsky group at University of Illinois at Chicago developed a kinetics mechanism to predict a specific type of jet fuel (Jet-A, POSF 4658). The first attempt to model this fuel was done using a surrogate mixture of n-decane/iso-octane/toluene (1st generation). However, a second-generation surrogate was developed which contains 40.4/29.5/22.8/7.3 of n-dodecane/iso-octane/n-propylbenzene/1,3,5-trimethylbezene by volume. The detailed mechanism contains 2080 species and 8310 reactions. Figure 37 compares ignition delay time predictions from this mechanism and the experimental data for Jet-A in air. At 10 atm, the mechanism accurately predicts the ignition at the higher-temperature region. Moreover, at 20 atm, the mechanism shows precise predictions of shorter ignition delay times (less than 500 µs), then an over-prediction of the longer ignition delay times is observed. However, the prediction from this mechanism was performed at a constant pressure, while there is a small pressure increase over time (dp/dt) which could artificially shorten the ignition delay times at longer test times.

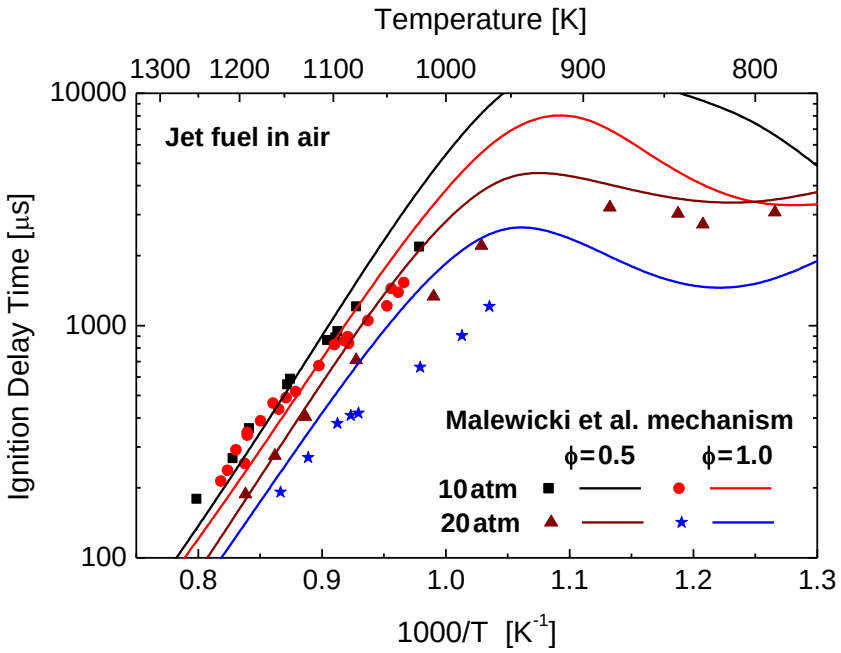

Figure 37: Prediction from the Malewicki et al. mechanism for jet fuel in air for 10 and 20 atm, and ϕ = 0.5 and 1.0 [47].

Narayanaswamy [46] collaborated with the Institute for Combustion Technology at Aachen University to develop a jet fuel surrogate which contains n-dodecane, methylcyclohexane, and m-xylene along with a chemical kinetics mechanism that contains 369 species and 2691 reactions. The mechanism was assembled based on several previous models. The basic model used to build this mechanism is a C_0-C_4 model combined with other sub-mechanisms previously published by the same authors for n-dodecane and methylcyclohexane [50-53]. Figure 38 shows the ignition delay time predictions from this mechanism for jet fuel in air at pressures of 10 and 20 atm and equivalence ratios of 0.5 and 1.0. The ignition delay time predictions yielded satisfactory results at the high-temperature region considering the uncertainty in the experimental measurements. However, at 20 atm and an equivalence ratio of 0.5, the mechanism over predicts the ignition delay time at the negative-temperature-coefficient region (less than 900 K).

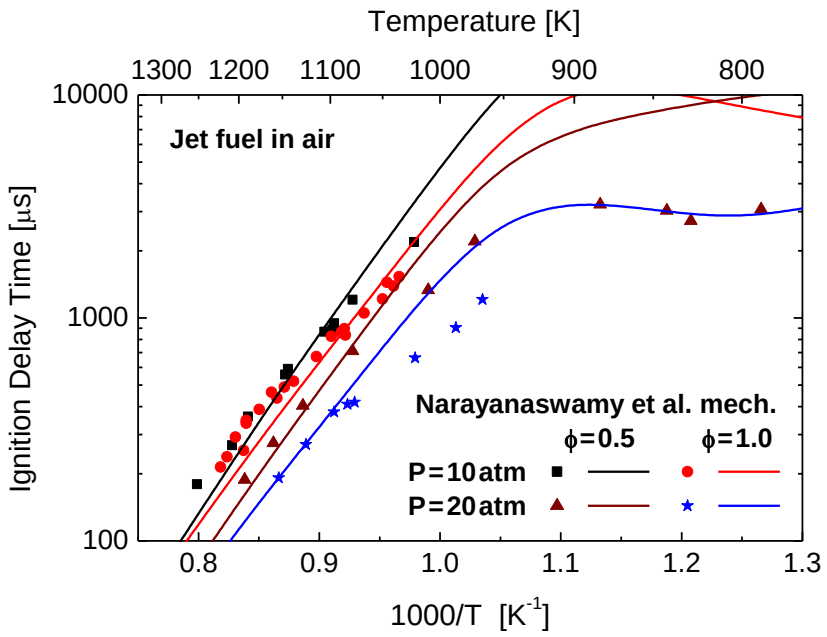

Figure 38: Prediction from the Narayanaswamy et al. mechanism for jet fuel in air for 10 and 20 atm, and ϕ=0.5 and 1.0 [46].

Direct comparison of the three jet fuel kinetics mechanisms at a pressure of 20 atm and an equivalence ratio of 0.5 is shown in Figure 39. The Narayanaswamy et al. and Malewicki et al. mechanisms capture the high-temperature region of above 1100 K accurately within the experimental uncertainty, while the Honnet et al. mechanism under predicts the ignition delay time for that region. On the other hand, the Honnet et al. mechanism captures the ignition delay time for the intermediate temperature region of 900-1100 K region accurately. For the low-temperature region (less than 900 K), the Malewicki et al. mechanism produces the best prediction capturing the general trend of the ignition delay times in that region. Overall, Malewicki et al. mechanisms produced the best results considering that these simulations were conducted at a constant pressure while shock-tube experiments are prone to gas dynamic effects which create an increase in pressure over time. This increasing pressure (and hence temperature) over time leads to artificially shorter ignition, especially for experiments of longer test times. However, this mechanism is computationally expensive due to the large number of reactions.

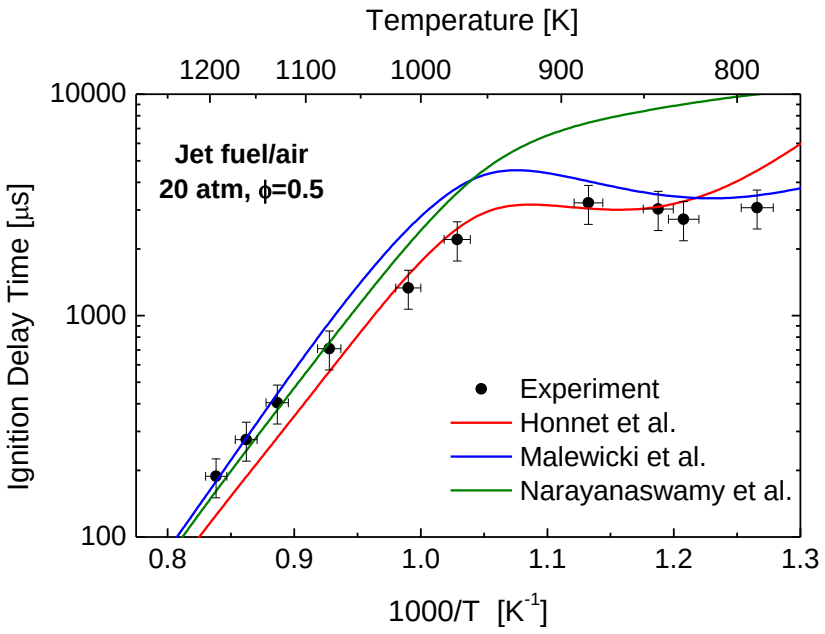

Figure 39: Comparison of kinetics mechanisms for jet fuel/air at 20 atm and ϕ=0.5 [45-47].

3.7.2 Diesel Fuel Mechanisms

Pei et al. [35] in collaboration with the Lawrence Livermore National Laboratory developed a chemical kinetics mechanism tailored for a surrogate fuel to represent the combustion chemistry of diesel fuels. They used a surrogate consisting of 77% n-dodecane and 23% m-xylene by volume. The mechanism is a reduced model that contains 163 species and 887 reactions, and it was developed based on a previous detailed model that contains 2885 species and 11,754 reactions. Figure 40 shows the prediction from this mechanism for diesel fuel in air at pressures of 10 and 20 atm and equivalence ratios of 0.5 and 1.0. The predictions produced very good results when compared with the experimental data. At 10 atm, the predictions were accurate in capturing the convergence of the two equivalence ratios at higher temperatures. In addition, at 20 atm and an equivalence ratio of 0.5, the mechanism predictions of the negative-temperature-coefficient region were within the uncertainty of the experimental measurements.

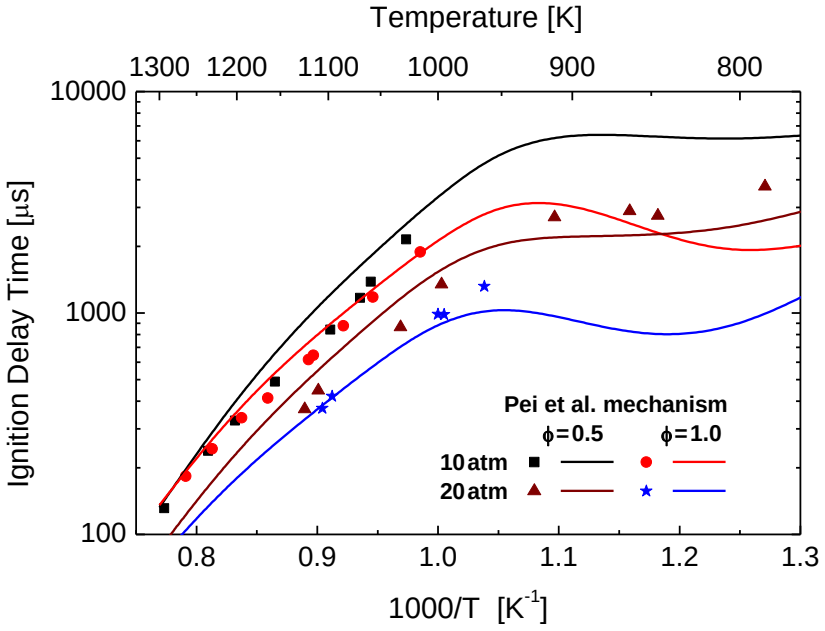

Figure 40: Prediction from the Pei et al. (LLNL) mechanism for jet fuel in air for 10 and 20 atm and ϕ = 0.5 and 1.0 [35].

Frassoldati et al. [49] from the CRECK modeling group (Politecnico Milano) developed a skeletal chemical kinetics mechanism for diesel fuel that contains 123 species and 1017 reactions. This mechanism is a reduced model from a lumped model that consisted of 451 species and 17,747 reactions. They used a surrogate mixture of n-decane and α-methylnaphthalene to represent the diesel fuel. The prediction from this mechanism for diesel fuel in air at 10 and 20 atm, and equivalence ratios of 0.5 and 1.0 is shown in Figure 41. At 10 atm and an equivalence ratio of 1.0, the model shows satisfactory prediction for the shorter ignition delay times of less than 1000 μs. However, for all the other cases, the model over-predict the ignition delay times. In addition, the model captures the trend at the negative-temperature coefficient region but over-predicts the ignition delay times.

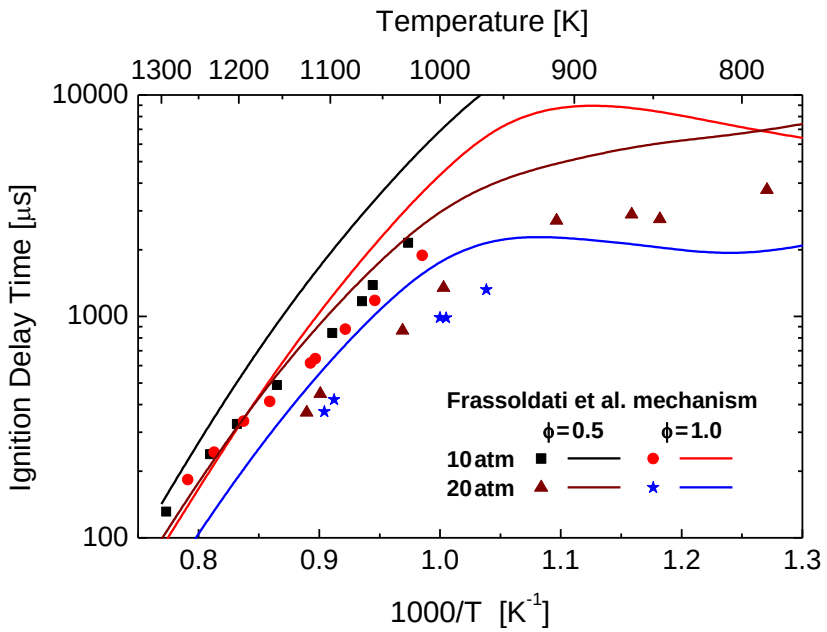

Figure 41: Prediction from the Frassoldati et al. mechanism for jet fuel in air for 10 and 20 atm and ϕ = 0.5 and 1.0 [49].

Yao et al. [48] from the Center for Combustion Energy (Tsinghua University, China) developed a compact skeletal mechanism for a single surrogate model (n-dodecane) to represent the combustion chemistry of diesel fuels. This mechanism was tailored to represent the combustion of diesel fuel at the low-temperature region and consists of 54 species 269 reactions. This mechanism was built on a previous detailed mechanism for n-dodecane from the University of Southern California [54]. Figure 42 shows the predictions of ignition delay times at 10 and 20 atm and equivalence ratios of 0.5 and 1.0. The model shows satisfactory predictions for the stoichiometric condition at 20 atm. However, for the higher-temperature region (above 1150 K), the model under-predicts the ignition delay time at 10 atm for both equivalence ratios and over-predicts the ignition delay time at 20 atm and an equivalence ratio of 0.5. On the other hand, this model remarkably captures the negative-temperature region at 20 atm and equivalence ratio of 0.5.

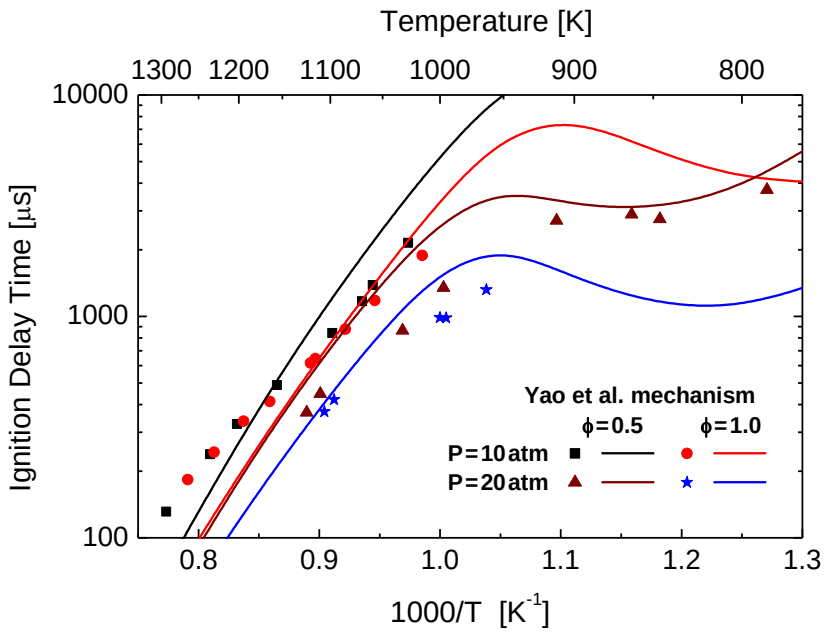

Figure 42: Prediction from the Yao et al. mechanism for jet fuel in air for 10 and 20 atm and ϕ = 0.5 and 1.0 [48].

Figure 43 shows a comparison of the three diesel fuel mechanisms discussed above at 20 atm and an equivalence ratio of 0.5. The mechanism of Frassoldati et al. over-predicts the ignition delay time for the entire range of current data. On the other hand, both the mechanisms of Pei et al. and Yao et al. capture the negative-temperature-coefficient region well within the uncertainty of the experimental measurements. However, the mechanism of Pei et al. yielded a better prediction for the higher-temperature region, capturing the ignition delay times accurately.

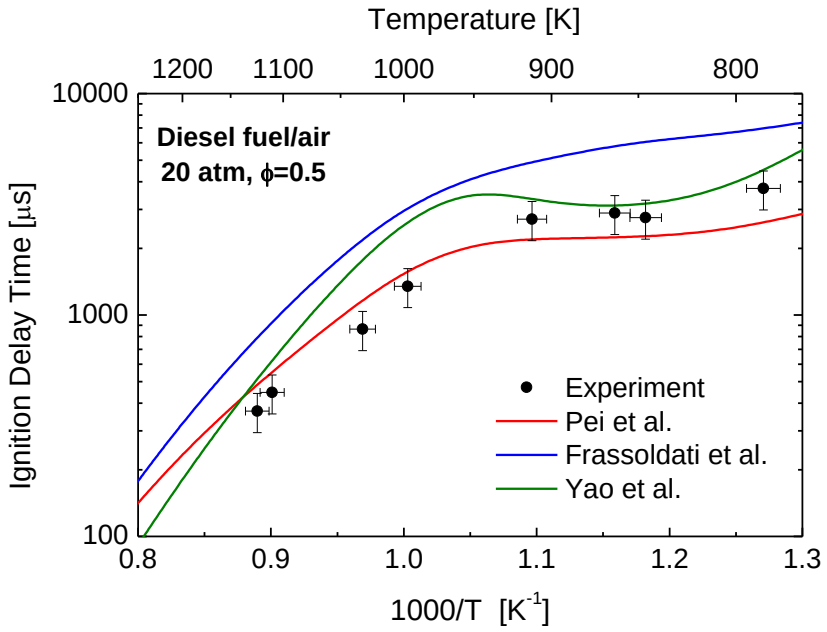

Figure 43: Comparison of kinetics mechanisms for diesel fuel/air at 20 atm and ϕ = 0.5 [35, 48, 49].

CHAPTER IV

CONCLUSION AND FUTURE WORK

Ignition delay time measurements for Jet-A, RP-1, and DF-2 in air were obtained using the high-pressure shock tube facility at Texas A&M University. These liquid fuels have low-vapor pressure, and a new heating system was utilized to allow shock-tube, gas-phase experiments. The measurements were conducted at elevated temperatures and pressures to mimic practical engine conditions. The experiments were performed at 10 and 20 atm, and a temperature range of 785 to 1293 K for two equivalence ratios, $\phi = 0.5$ and 1.0. Endwall pressure and OH* emission signals allowed accurate definition of ignition delay times. The ignition delay times had low scatter and were in excellent agreement with previously published data when comparisons were possible. Longer test times (above 2500 μs) were obtained via driver gas-tailoring method to explore the NTC regime for the three fuels. To the author's knowledge, this thesis reports the first shock-tube ignition delay times for RP-1 fuel and expands the reported data for DF-2 to a broader range of conditions while confirming the archival results for Jet-A.

Correlations to accurately predict the high-temperature ignition delay times of the three fuels were presented. The correlations were obtained via multiple linear regression analysis of the experimental data with three independent variables of pressure, equivalence ratio, and temperature. Pressure scaling factors were provided for each fuel and performed well to scale ignition delay times from other groups.

Prediction from several chemical kinetics mechanisms for jet and diesel fuels were obtained and compared to the experimental measurements. For jet fuel, the mechanism predictions from Honnet et al. [45], Malewicki et al. [47], and Narayanaswamy et al. [46] were conducted using different surrogate mixtures. Overall, the predictions of Malewicki et al. yielded the best

results to represent the ignition delay time of Jet-A. On the other hand, the mechanisms of Pei et al. [35], Frassoldati et al. [49], and Yao et al. [48], were utilized to model the ignition delay times of diesel fuel. The mechanism of Pei et al. remarkably captures the ignition delay time of DF-2 over the experimental range of conditions obtained in this study.

Future work should aim to explore a broader range of conditions for these fuels. Several studies have shown that the high-temperature ignition delay times of multicomponent fuels typically fall in the same region. However, differences in ignition times were observed in the NTC and lower-temperature regimes. Further investigations to explore these regimes are necessary to provide validation targets for liquid fuel kinetics mechanisms. In addition, time history absorption measurements for single species concentrations, such as H_2O and OH, can be used for validation of kinetics mechanisms.

REFERENCES

[1] U.S. Energy Information Administration, International Energy Outlook 2017, Available: eia.gov/outlooks/ieo/pdf/0484(2017).pdf.

[2] M. Colket, J. Heyne, M. Rumizen, M. Gupta, T. Edwards, W.M. Roquemore, G. Andac, R. Boehm, J. Lovett, R. Williams, J. Condevaux, D. Turner, N. Rizk, J. Tishkoff, C. Li, J. Moder, D. Friend, V. Sankaran, Overview of the National Jet Fuels Combustion Program, AIAA Journal 55 (2017) 1087-1104.

[3] J.T. Edwards, Reference Jet Fuels for Combustion Testing in: 55th AIAA Aerospace Sciences Meeting, American Institute of Aeronautics and Astronautics, 2017, pp. AIAA 2017-0146.

[4] R. Xu, K. Wang, S. Banerjee, J. Shao, T. Parise, Y. Zhu, S. Wang, A. Movaghar, D.J. Lee, R. Zhao, X. Han, Y. Gao, T. Lu, K. Brezinsky, F.N. Egolfopoulos, D.F. Davidson, R.K. Hanson, C.T. Bowman, H. Wang, A physics-based approach to modeling real-fuel combustion chemistry – II. Reaction kinetic models of jet and rocket fuels, Combustion and Flame (2018) 0010-2180.

[5] A.J. Dean, O.G. Penyazkov, K.L. Sevruk, B. Varatharajan, Autoignition of surrogate fuels at elevated temperatures and pressures, Proceedings of the Combustion Institute 31 (2007) 2481-2488.

[6] S.S. Vasu, D.F. Davidson, R.K. Hanson, Jet fuel ignition delay times: Shock tube experiments over wide conditions and surrogate model predictions, Combustion and Flame 152 (2008) 125-143.

[7] K. Kumar, C.-J. Sung, An experimental study of the autoignition characteristics of conventional jet fuel/oxidizer mixtures: Jet-A and JP-8, Combustion and Flame 157 (2010) 676-685.

[8] H. Wang, M.A. Oehlschlaeger, Autoignition studies of conventional and Fischer–Tropsch jet fuels, Fuel 98 (2012) 249-258.

[9] V.P. Zhukov, V.A. Sechenov, A.Y. Starikovskiy, Autoignition of kerosene (Jet-A)/air mixtures behind reflected shock waves, Fuel 126 (2014) 169-176.

[10] D.F. Davidson, Y. Zhu, J. Shao, R.K. Hanson, Ignition delay time correlations for distillate fuels, Fuel 187 (2017) 26-32.

[11] A.R. De Toni, M. Werler, R.M. Hartmann, L.R. Cancino, R. Schießl, M. Fikri, C. Schulz, A.A.M. Oliveira, E.J. Oliveira, M.I. Rocha, Ignition delay times of Jet A-1 fuel:

Measurements in a high-pressure shock tube and a rapid compression machine, Proceedings of the Combustion Institute 36 (2017) 3695-3703.

[12] S. Burden, A. Tekawade, M.A. Oehlschlaeger, Ignition delay times for jet and diesel fuels: Constant volume spray and gas-phase shock tube measurements, Fuel 219 (2018) 312-319.

[13] J. Shao, Y. Zhu, S. Wang, D.F. Davidson, R.K. Hanson, A shock tube study of jet fuel pyrolysis and ignition at elevated pressures and temperatures, Fuel 226 (2018) 338-344.

[14] Y. Zhu, S. Li, D.F. Davidson, R.K. Hanson, Ignition delay times of conventional and alternative fuels behind reflected shock waves, Proceedings of the Combustion Institute 35 (2015) 241-248.

[15] T. Edwards, Liquid Fuels and Propellants for Aerospace Propulsion: 1903-2003, Journal of Propulsion and Power 19 (2003) 1089-1107.

[16] M.L. Huber, E.W. Lemmon, L.S. Ott, T.J. Bruno, Preliminary Surrogate Mixture Models for the Thermophysical Properties of Rocket Propellants RP-1 and RP-2, Energy & Fuels 23 (2009) 3083-3088.

[17] D.F. Davidson, J. Shao, T. Parise, R.K. Hanson, Shock Tube Measurements of Jet and Rocket Fuel Ignition Delay Times in: 55th AIAA Aerospace Sciences Meeting, American Institute of Aeronautics and Astronautics, 2017.

[18] C. Zhang, B. Li, F. Rao, P. Li, X. Li, A shock tube study of the autoignition characteristics of RP-3 jet fuel, Proceedings of the Combustion Institute 35 (2015) 3151-3158.

[19] H.H. Wolfer, Ignition lag in diesel engines, translated by royal air craft establishment, Farnborough Library, No. 358, UDC 621-436.047 (1938).

[20] S.-I. Kwon, M. Arai, H. Hiroyasu, in: SAE International: 1991.

[21] A.A. Aradi, T.W. Ryan, in: SAE International: 1995.

[22] M. Lapuerta, J. Sanz-Argent, R.R. Raine, Ignition Characteristics of Diesel Fuel in a Constant Volume Bomb under Diesel-Like Conditions. Effect of the Operation Parameters, Energy & Fuels 28 (2014) 5445-5454.

[23] K. Miwa, T. Ohmija, T. Nishitani, A Study of the Ignition Delay of Diesel Fuel Spray Using a Rapid Compression Machine, JSME international journal. Ser. 2, Fluids engineering, heat transfer, power, combustion, thermophysical properties 31 (1988) 166-173.

[24] S. Kobori, T. Kamimoto, A.A. Aradi, A study of ignition delay of diesel fuel sprays, International Journal of Engine Research 1 (2000) 29-39.

[25] L.J. Spadaccini, J.A. Tevelde, Autoignition characteristics of aircraft-type fuels, Combustion and Flame 46 (1982) 283-300.

[26] D.R. Haylett, D.F. Davidson, R.K. Hanson, Ignition delay times of low-vapor-pressure fuels measured using an aerosol shock tube, Combustion and Flame 159 (2012) 552-561.

[27] D.R. Haylett, P.P. Lappas, D.F. Davidson, R.K. Hanson, Application of an aerosol shock tube to the measurement of diesel ignition delay times, Proceedings of the Combustion Institute 32 (2009) 477-484.

[28] S. Gowdagiri, W. Wang, M.A. Oehlschlaeger, A shock tube ignition delay study of conventional diesel fuel and hydroprocessed renewable diesel fuel from algal oil, Fuel 128 (2014) 21-29.

[29] O.G. Penyazkov, K.L. Sevrouk, V. Tangirala, N. Joshi, Autoignitions of Diesel Fuel/Air Mixtures Behind Reflected Shock Waves, Proceedings of the European Combustion Meeting 2009 (2009).

[30] G. Kukkadapu, C.-J. Sung, Autoignition study of ULSD#2 and FD9A diesel blends, Combustion and Flame 166 (2016) 45-54.

[31] C.J. Aul, W.K. Metcalfe, S.M. Burke, H.J. Curran, E.L. Petersen, Ignition and kinetic modeling of methane and ethane fuel blends with oxygen: A design of experiments approach, Combustion and Flame 160 (2013) 1153-1167.

[32] A.R. Amadio, M.W. Crofton, E.L. Petersen, Test-time extension behind reflected shock waves using CO2–He and C3H8–He driver mixtures, Shock Waves 16 (2006) 157-165.

[33] A. Burcat, B. Ruscic, Extended third millenium ideal gas and condensed phase thermochemical database for combustion with updates from active thermochemical tables, http://garfield.chem.elte.hu/Burcat/burcat.html (2011).

[34] M.E. MacDonald, D. Davidson, R.K. Hanson, Decomposition Measurements of RP-1, RP-2, JP-7, n-Dodecane, and Tetrahydroquinoline in Shock Tubes, Journal of Propulsion and Power 27 (2011) 981-989.

[35] Y. Pei, M. Mehl, W. Liu, T. Lu, W.J. Pitz, S. Som, A Multicomponent Blend as a Diesel Fuel Surrogate for Compression Ignition Engine Applications, Journal of Engineering for Gas Turbines and Power 137 (2015) 111502-111502-9.

[36] R. Rebagay, Heated Shock Tube Design and Characterization for Liquid Fuel Combustion Experiments, M.S. thesis, Texas A&M University (2017).

[37] T. Kathrotia, M. Fikri, M. Bozkurt, M. Hartmann, U. Riedel, C. Schulz, Study of the H+O+M reaction forming OH∗: Kinetics of OH∗ chemiluminescence in hydrogen combustion systems, Combustion and Flame 157 (2010) 1261-1273.

[38] J.T. Edwards, Properties for rocket and diesel fuels, privately communicated (2018).

[39] J. Herzler, M. Fikri, K. Hitzbleck, R. Starke, C. Schulz, P. Roth, G.T. Kalghatgi, Shock-tube study of the autoignition of n-heptane/toluene/air mixtures at intermediate temperatures and high pressures, Combustion and Flame 149 (2007) 25-31.

[40] D.C. Horning, D.F. Davidson, R.K. Hanson, Study of the High-Temperature Autoignition of n-Alkane/O/Ar Mixtures, Journal of Propulsion and Power 18 (2002) 363-371.

[41] J.M. Hall, M.J.A. Rickard, E.L. Petersen, COMPARISON OF CHARACTERISTIC TIME DIAGNOSTICS FOR IGNITION AND OXIDATION OF FUEL/OXIDIZER MIXTURES BEHIND REFLECTED SHOCK WAVES, Combustion Science and Technology 177 (2005) 455-483.

[42] D.F. Davidson, S.C. Ranganath, K.Y. Lam, M. Liaw, Z. Hong, R.K. H, Ignition Delay Time Measurements of Normal Alkanes and Simple Oxygenates, Journal of Propulsion and Power 26 (2010) 280-287.

[43] J. He, K. Yong, W. Zhang, P. Li, C. Zhang, X. Li, Shock Tube Study of Ignition Delay Characteristics of n-Nonane and n-Undecane in Argon, Energy & Fuels 30 (2016) 8886-8895.

[44] M.L. Huber, E.W. Lemmon, T.J. Bruno, Surrogate Mixture Models for the Thermophysical Properties of Aviation Fuel Jet-A, Energy & Fuels 24 (2010) 3565-3571.

[45] S. Honnet, K. Seshadri, U. Niemann, N. Peters, A surrogate fuel for kerosene, Proceedings of the Combustion Institute 32 (2009) 485-492.

[46] K. Narayanaswamy, H. Pitsch, P. Pepiot, A component library framework for deriving kinetic mechanisms for multi-component fuel surrogates: Application for jet fuel surrogates, Combustion and Flame 165 (2016) 288-309.

[47] T. Malewicki, S. Gudiyella, K. Brezinsky, Experimental and modeling study on the oxidation of Jet A and the n-dodecane/iso-octane/n-propylbenzene/1,3,5-trimethylbenzene surrogate fuel, Combustion and Flame 160 (2013) 17-30.

[48] T. Yao, Y. Pei, B.-J. Zhong, S. Som, T. Lu, K.H. Luo, A compact skeletal mechanism for n-dodecane with optimized semi-global low-temperature chemistry for diesel engine simulations, Fuel 191 (2017) 339-349.

[49] A. Frassoldati, A. Cuoci, A. Stagni, T. Faravelli, E. Ranzi, Skeletal kinetic mechanism for diesel combustion, Combustion Theory and Modelling 21 (2017) 79-92.

[50] G. Blanquart, P. Pepiot-Desjardins, H. Pitsch, Chemical mechanism for high temperature combustion of engine relevant fuels with emphasis on soot precursors, Combustion and Flame 156 (2009) 588-607.

[51] K. Narayanaswamy, G. Blanquart, H. Pitsch, A consistent chemical mechanism for oxidation of substituted aromatic species, Combustion and Flame 157 (2010) 1879-1898.

[52] K. Narayanaswamy, P. Pepiot, H. Pitsch, A chemical mechanism for low to high temperature oxidation of n-dodecane as a component of transportation fuel surrogates, Combustion and Flame 161 (2014) 866-884.

[53] K. Narayanaswamy, H. Pitsch, P. Pepiot, A chemical mechanism for low to high temperature oxidation of methylcyclohexane as a component of transportation fuel surrogates, Combustion and Flame 162 (2015) 1193-1213.

[54] X. You, F.N. Egolfopoulos, H. Wang, Detailed and simplified kinetic models of n-dodecane oxidation: The role of fuel cracking in aliphatic hydrocarbon combustion, Proceedings of the Combustion Institute 32 (2009) 403-410.

[55] M. Alrefae, E.-t. Es-sebbar, A. Farooq, Absorption cross-section measurements of methane, ethane, ethylene and methanol at high temperatures, Journal of Molecular Spectroscopy 303 (2014) 8-14.

APPENDIX A

IGNITION DELAY TIME EXPERIMENTS DATA

Table A-1: Ignition delay time experiments data for n-Pentane

n-Pentane/4%O_2/Ar, phi=1.0: C_5H_{12}=0.5%, O_2=4.0%, Ar=95.5%					
P_1 (torr)	T_1 (°C)	V_s (mm/μs)	T_5 (K)	P_5 (atm)	τ_{ign}
60.09	68.6	0.7794	1386	1.812	423
64.16	69.7	0.7624	1335	1.801	792
58.22	70.1	0.7373	1261	1.473	2351
58.38	69.8	0.7922	1426	1.838	357
59.07	69.7	0.7754	1374	1.745	594
66.16	69.7	0.7570	1319	1.818	1102
70.06	69.5	0.7426	1276	1.817	2259
68.07	69.4	0.7433	1278	1.771	1659
56.06	69.3	0.7917	1425	1.766	300
54.06	69.4	0.7999	1450	1.755	257
52	69.5	0.7605	1329	1.45	941
50.58	69.6	0.8180	1508	1.753	129

Table A-2: Ignition delay time experiments data for n-Octane

n-Octane/4%O_2/Ar, phi=1.0: C_8H_{18}=0.32%, O_2=4.0%, Ar=95.68%					
P_1 (torr)	T_1 (°C)	V_s (mm/μs)	T_5 (K)	P_5 (atm)	τ_{ign}
83.42	89.2	0.7720	1375	2.253	471
85.41	89.2	0.7620	1345	2.216	653
87.46	88.9	0.7577	1332	2.233	750
89.58	89.1	0.754	1321	2.251	767
94.33	89.1	0.7402	1280	2.239	1216
92.11	89.3	0.7487	1305	2.263	978
82.37	89.3	0.7755	1386	2.254	378
80.51	89.3	0.7786	1396	2.23	306
89.82	90.8	0.7518	1315	2.221	928
78.9	90.6	0.7761	1388	2.153	366
76.68	80.2	0.7929	1440	2.236	177
83.7	89.9	0.7495	1308	2.058	1011
77.3	89.8	0.7748	1384	2.106	411

Table A-3: Ignition delay time experiments data for n-Nonane

n-Nonane/4%O_2/Ar, phi=1.0: C_9H_{20}=0.286%, O_2=4.0%, Ar=95.714%					
P_1 (torr)	T_1 (°C)	V_s (mm/μs)	T_5 (K)	P_5 (atm)	τ_{ign}
61.43	89.3	0.7820	1406	1.726	354
63.16	89.3	0.7821	1406	1.775	395
64.44	89.3	0.7299	1250	1.464	2330
62.29	89.3	0.7835	1410	1.816	390
78.08	89	0.7945	1445	2.306	258
85.06	88.8	0.7609	1341	2.203	747
83.09	88.7	0.7521	1315	2.077	1020
59.01	78.0	0.7974	1448	1.841	277
67.99	68.2	0.7498	1298	1.836	1491
60.01	75.1	0.7743	1375	1.735	578
59.8	68.0	0.7658	1346	1.724	707
57.25	66.6	0.7848	1404	1.787	487
70.65	67.8	0.7316	1245	1.773	2437
64.84	64.6	0.7727	1366	1.858	661
64.04	69.9	0.7576	1322	1.772	1060
66.1	69.7	0.7549	1314	1.811	1257
68.04	69.7	0.7450	1285	1.791	1537
58	69.6	0.7796	1389	1.752	503
67.04	76.4	0.7704	1364	1.899	682

Table A-4: Ignition delay time experiment data for Jet-A (phi=1.0)

Jet-A/air, phi=1.0: $C_{11.4}H_{22.1}$=1.224%, O_2=20.751%, N_2=78.025% (Jet-A POSF#10325)					
P_1 (torr)	T_1 (°C)	V_s (mm/μs)	T_5 (K)	P_5 (atm)	τ_{ign}
211	89.3	0.9747	1138	11.049	467
199.6	89.7	0.9813	1148	10.651	457
229.6	89.7	0.9411	1086	10.756	828
185.3	90.6	0.9896	1162	10.114	458
191.4	110.2	1.0016	1194	10.066	253
182.1	110.9	1.0142	1214	9.93	240
174.7	111.0	1.0193	1222	9.672	222
239.7	111.3	0.9401	1099	10.289	802
245.2	111.4	0.9048	1046	9.312	1561
210.4	112.8	0.9896	1176	10.557	367
215.4	109.3	0.9781	1156	12.336	348
251.3	110.1	0.9338	1089	10.611	806
225.1	110.7	0.9501	1114	10.017	670
283.8	111.0	0.9005	1040	10.633	1301
272.4	111.9	0.8967	1035	10.033	1532
239	112.7	0.9180	1067	9.462	1121
184.4	112.7	0.9303	1085	7.614	1140
190.9	112.8	0.9989	1191	9.863	342
181.1	112.8	0.9987	1191	9.35	373
164.8	113.0	1.0073	1204	8.733	338
296.9	112.1	0.9089	1050	11.501	1053
587.3	104.7	0.9280	1076	24.825	332
491	111.7	0.9758	1154	23.675	160
541.6	111.0	0.9570	1125	24.63	216
681.9	144.3	0.9234	1096	24.458	305
900.5	134.2	0.8386	966	24.443	974
864.6	133.0	0.8539	987	25.033	710
770.8	130.2	0.8788	1021	24.79	525
678.6	131.9	0.9207	1083	25.226	319

Table A-5: Ignition delay time experiment data for Jet-A (phi=0.5)

Jet-A/air, phi=0.5: $C_{11.4}H_{22.1}$=0.616%, O_2=20.870%, N_2=78.505% (Jet-A POSF#10325)					
P_1 (torr)	T_1 (°C)	V_s (mm/μs)	T_5 (K)	P_5 (atm)	τ_{ign}
200.4	109.7	1.0113	1252	9.92	181
221	109.0	0.9854	1208	10.123	265
271.3	109.5	0.9229	1106	10.099	857
246.4	109.1	0.9470	1144	9.966	592
262.7	112.9	0.9472	1147	10.478	530
314.5	112.8	0.9154	1096	11.264	833
304.8	113.0	0.9168	1098	10.961	804
348.6	110.3	0.8696	1022	10.695	2044
282.1	112.9	0.9044	1078	9.718	1233
220.5	112.7	0.9727	1189	9.563	379
525.8	96.4	0.9816	1193	24.978	148
595	94.4	0.9429	1128	25.145	316
807.4	95.3	0.8675	1010	26.117	1001
708.6	102.1	0.9083	1078	25.819	539
919.5	104.2	0.8393	972	25.767	1680
645.3	143.6	0.9426	1160	22.619	241
1289	110.1	0.7094	790	20	3081
1153	112.1	0.7363	828	20.172	2699
1055	112.8	0.7460	842	19.247	3159
943.6	112.7	0.7745	883	19.56	3311

Table A-6: Ignition delay time experiment data for RP-1 (phi=1.0)

RP-1/air, phi=1.0: $C_{12.0}H_{24.1}$=1.1521%, O_2=20.7664%, N_2=78.0815% (RP-1 POSF#5235)					
P_1 (torr)	T_1 (°C)	V_s (mm/μs)	T_5 (K)	P_5 (atm)	τ_{ign}
208.4	112.8	0.9717	1153	9.77	477
258.7	120.1	0.9386	1106	10.575	688
204	120.9	1.0011	1204	10.189	296
173.6	121.0	1.0378	1264	9.694	175
303.8	119.6	0.9026	1052	10.977	1039
322	120.3	0.8754	1013	10.509	1534
281.2	121.5	0.9238	1085	10.868	776
250	121.9	0.9436	1115	10.324	648
727.3	129.9	0.8810	1025	24.044	557
772.5	130.2	0.8670	1005	24.233	656
672.7	130.4	0.9042	1060	24.113	454
575.5	131.5	0.9400	1115	23.224	283
479.1	131.4	0.9757	1170	21.731	197
847.1	131.8	0.8465	976	24.447	848

Table A-7: Ignition delay time experiment data for RP-1 (phi=0.5)

RP-1/air, phi=0.5: $C_{12.0}H_{24.1}$=0.5794%, O_2=20.8867%, N_2=78.5339% (RP-1 POSF#5235)					
P_1 (torr)	T_1 (°C)	V_s (mm/μs)	T_5 (K)	P_5 (atm)	τ_{ign}
214	121.4	0.9973	1239	9.659	223
319.3	121.7	0.9015	1082	10.461	1058
359	120.8	0.8651	1024	10.33	2141
253.7	120.3	0.9533	1164	9.982	455
286.5	120.6	0.9088	1093	9.673	1014
271	121.0	0.9155	1103	9.353	886
321.1	121.1	0.8912	1065	10.158	1258
231.3	120.5	0.9738	1199	9.723	343
279.6	121.2	0.9309	1128	10.169	637
338.3	121.5	0.8850	1056	10.451	1333
728.4	129.9	0.9234	1122	25.344	307
807.7	131.0	0.8884	1066	24.745	511
652.4	131.6	0.9431	1155	24.111	229
945.8	129.7	0.8544	1013	25.678	849
1065	129.9	0.8308	977	26.372	1380
854.3	118.1	0.7714	882	17.371	3633
1074	117.1	0.7029	785	16.012	4136
1084	118.0	0.7529	885	20.331	3375

Table A-8: Ignition delay time experiment data for DF-2 (phi=1.0)

DF-2/air, phi=1.0: $C_{13.1}H_{24.0}$=1.0879%, O_2=20.7798%, N_2=78.1322% (DF-2 POSF#12758)					
P_1 (torr)	T_1 (°C)	V_s (mm/μs)	T_5 (K)	P_5 (atm)	τ_{ign}
199.5	121.6	1.0074	1230	9.851	247
254.6	121.6	0.9388	1120	10.07	612
288.6	128.4	0.9132	1085	10.185	860
334.7	129.2	0.8662	1015	9.919	1896
311.1	130.0	0.8939	1057	10.185	1168
239	130.7	0.9318	1115	8.922	719
221.5	131.0	0.9815	1194	9.743	345
236.2	130.9	0.9629	1164	9.783	422
180.2	131.1	1.0245	1264	9.063	201
592	133.1	0.9251	1106	21.404	348
660	134.4	0.9177	1096	23.142	366
876.9	135.1	0.8278	963	21.869	1211
698.6	125.3	0.8581	1000	20.379	970
663.7	127.6	0.8534	995	17.995	1093

Table A-9: Ignition delay time experiment data for DF-2 (phi=0.5)

DF-2/air, phi=0.5: $C_{13.1}H_{24.0}$=0.5470%, O_2=20.8935%, N_2=78.5596% (DF-2 POSF#12758)					
P_1 (torr)	T_1 (°C)	V_s (mm/μs)	T_5 (K)	P_5 (atm)	τ_{ign}
261.4	129.5	0.9667	1202	10.266	318
378.4	130.2	0.8799	1059	10.933	1266
349.2	130.6	0.8855	1069	10.284	1143
319.9	130.8	0.9039	1098	10.061	837
274.2	131.1	0.9391	1156	9.735	502
202.9	131.1	1.0200	1293	9.339	140
402.2	131.4	0.8586	1027	10.678	2016
234	131.4	0.9860	1235	9.68	246
872	132.5	0.8615	1032	23.309	746
733.1	133.1	0.9039	1110	22.858	393
978.1	133.3	0.8384	997	23.833	1158
680.1	130.6	0.9198	1124	22.639	327
1009.1	135.0	0.7812	912	19.266	2826
1180	133.7	0.7478	863	19.498	2965
1265	124.5	0.7402	846	20.958	2635
1364	127.0	0.6969	787	18.116	4101

APPENDIX B

METHANE ABSORPTION MEASUREMENTS

This appendix is to document absorption cross-section measurements made in the shock tube using a He-Ne laser at 3.39 μm for a mixture of 1% CH_4 in Ar. The measurements were made at a room temperature of 298 K.

P [torr]	σ [cm/molecule]	P [torr]	σ [cm/ molecule]	P [torr]	σ [cm/ molecule]
50.2	2.64136E-18	300.3	7.38968E-19	699.6	3.94319E-19
74.9	2.1175E-18	350.3	6.48153E-19	749.9	3.79329E-19
100.1	1.72948E-18	400.1	5.79476E-19	760	3.76603E-19
125.1	1.46787E-18	450.3	5.3164E-19	799.9	3.67294E-19
150.3	1.29671E-18	500.3	4.93157E-19	849.6	3.5416E-19
175.4	1.14821E-18	549.6	4.58865E-19	900.1	3.46128E-19
200	1.03885E-18	600.4	4.33699E-19	950.1	3.37698E-19
250.4	8.55796E-19	649.9	4.10594E-19	1000.6	3.30978E-19

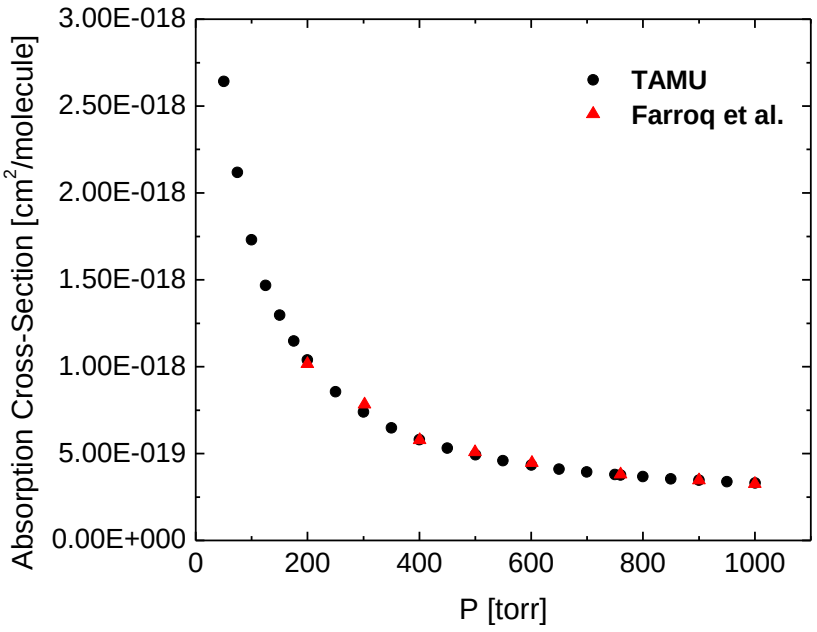

Figure 44: Absorption cross-section measurements for 1%CH_4/Ar at 298 K [55].